bioRxiv preprint doi: https://doi.org/10.1101/2022.10.04.510795; this version posted October 4, 2022. The copyright holder for this preprint (which was not certified by peer review) is the author/funder, who has granted bioRxiv a license to display the preprint in perpetuity. It is made available under aCC-BY-NC-ND 4.0 International license.

Molecular basis of the TRAP complex function in ER protein biogenesis

Mateusz Jaskolowski[1,4], Ahmad Jomaa[1,3,4,*], Martin Gamerdinger[2,4], Sandeep Shrestha[2], Marc Leibundgut[1], Elke Deuerling[2,*], Nenad Ban[1,*]

AFFLIATION:

[1] Department of Biology, Institute of Molecular Biology and Biophysics, ETH Zurich, 8093 Zurich, Switzerland.

[2] Department of Biology, Molecular Microbiology, University of Konstanz, 78457 Konstanz, Germany.

[3] Department of Molecular Physiology and Biological Physics and the Centre for Cell and Membrane Physiology, University of Virginia, 22903 Charlottesville, USA.

* Correspondence to: ban@mol.biol.ethz.ch (N.B.) ; elke.deuerling@uni-konstanz.de (E.D.); ahmadjomaa@virginia.edu (A.J.)

[4] These authors contributed equally: Mateusz Jaskolowski, Ahmad Jomaa, Martin Gamerdinger

ABSTRACT

The Translocon Associated Protein (TRAP) complex resides in the endoplasmic reticulum (ER) membrane and interacts with the Sec translocon and the translating ribosome to facilitate biogenesis of secretory and membrane proteins[1–4]. TRAP is essential for the secretion of many hormones, and its key role in the production of the hormone peptide insulin has been particularly well established[5,6]. The mechanism by which TRAP engages ribosomes and the translocon to facilitate translocation of protein clients in the secretory pathway is not clear. Here, we reveal the molecular architecture of the mammalian TRAP complex and how it engages the translating ribosome associated with Sec61 translocon on the ER membrane. The TRAP complex is anchored to the ribosome via a long tether and its position relative to the ribosome and the translocon is further stabilized by a finger-like loop. This spatial arrangement positions a cradle-like lumenal domain of TRAP below the protein conducting pore of the translocon for interactions with translocated nascent chains. The biological importance of these key interactions is evident by structure-guided TRAP mutations in *C. elegans* that lead to growth deficits associated with increased ER stress and defects in insulin secretion. Our findings elucidate the molecular basis of the TRAP complex in the biogenesis and translocation of proteins at the ER.

bioRxiv preprint doi: https://doi.org/10.1101/2022.10.04.510795; this version posted October 4, 2022. The copyright holder for this preprint (which was not certified by peer review) is the author/funder, who has granted bioRxiv a license to display the preprint in perpetuity. It is made available under aCC-BY-NC-ND 4.0 International license.

INTRODUCTION

Secretory and membrane proteins constitute one third of the human cell proteome[7] and are mostly co-translationally targeted to the endoplasmic reticulum (ER) to be translocated into the ER lumen or inserted into the ER membrane[8,9]. The membrane protein complex Sec61 acts as a protein-conducting pore to facilitate translocation of such proteins[10]. Referred to as Sec translocon, it is a heterotrimeric complex composed of α, β- and γ subunits, shaped like an hourglass with a central pore plugged by a hydrophobic helix that is displaced during protein translocation across the membrane, and a lateral gate where the two halves of the protein open to allow insertion of the newly synthesized polypeptide into the membrane[11,12].

To accommodate the diversity of proteins targeted to the ER, the Sec translocon interacts with different membrane protein complexes that aid in co-translational folding, assembly and processing of protein clients[13]. One of the key interactors with the Sec translocon is a highly abundant heterotetrameric transmembrane translocon-associated protein (TRAP) complex (harboring subunits TRAPα, TRAPβ, TRAPγ, TRAPδ) that also binds translating ribosomes and interacts with emerging nascent chains[1–4]. The TRAP complex is necessary for secretion and translocation of a subset of proteins including hormones like angiotensin or atrial natriuretic peptide, and the insulin-like growth factor 1 receptor[3,14]. TRAP-dependent clients are characterized by a signal sequence with a weaker gating activity[3], with a lower hydrophobicity and higher-than-average glycine and proline content in their signal sequence[14].

A recent study identified insulin as a bona fide client protein of TRAP, indicating that the TRAPα subunit is necessary for insulin biogenesis[5,6]. Previous analysis showed that the TRAP subunits become upregulated in pancreatic β cells when exposed to high concentration of glucose, presumably as a response to the requirement of insulin synthesis and secretion[15], and that a single-nucleotide mutation in the human TRAPα gene is linked with type 2 diabetes susceptibility[16]. Deletion of, or mutations in TRAP subunits lead to impaired ER function and are linked to various disorders, which further underscores the importance of TRAP in cargo translocation across the membrane[17–20]. Recent biochemical work showed that TRAP interactions with nascent chains and the translating ribosome precede interactions with the Sec translocon[6]. This presents the intriguing possibility that TRAP could also play a role in cargo handover from signal recognition particle (SRP) to the Sec translocon at the late stages of protein targeting[21].

Despite its important role in protein translocation across the ER membrane, the molecular basis of TRAP interaction with the ribosome and the Sec translocon are still not known. Here, we used single particle cryogenic electron microscopy (cryo-EM) combined with *in vivo* characterization to reveal the molecular basis of the interactions between the TRAP complex, the Sec translocon and a translating ribosome, which position TRAP for interactions with the nascent chain that emerges through the translocon pore. Our results describe a previously uncharacterized interaction between the C-terminal region of TRAPα with the ribosome. The structure also reveals the contact points between the TRAPα lumenal domain and the Sec

bioRxiv preprint doi: https://doi.org/10.1101/2022.10.04.510795; this version posted October 4, 2022. The copyright holder for this preprint (which was not certified by peer review) is the author/funder, who has granted bioRxiv a license to display the preprint in perpetuity. It is made available under aCC-BY-NC-ND 4.0 International license.

translocon, and shows the importance of hydrophobic residues within the TRAP lumenal domain, presumably important for folding of translocated proteins.

Structure of TRAP-Sec61 in complex with the translating ribosome

We reconstituted a protein targeting reaction to the ER membrane by incubating programmed ribosomes displaying an ER signal peptide (ribosome nascent chain complex, RNC) from rabbit reticulocyte lysate, together with canine SRP and pancreas EDTA and salt treated ER microsomes (EKRM)[22] **(Extended Data Fig. 1)**. The sample was then solubilized using mild detergents, purified and investigated using cryo-EM. We anticipated the formation of RNC complexes engaged with the Sec translocon and various accessory proteins that facilitate co-translational insertion and translocation of membrane and secretory proteins, respectively. 3D image classification resolved two complexes in the data, a ternary complex with RNC, TRAP, and Sec61, and a second complex additionally including the OST complex **(Extended Data Fig. 2)**. Since the atomic structure of the OST complex was recently reported[23] and its interactions with Sec61 were described[24], the OST containing complex is not further discussed here.

The three-dimensional reconstruction of the ternary complex revealed the translating ribosome with a large detergent micelle at the exit of the ribosomal tunnel **(Fig. 1a)**. The overall resolution of the reconstruction was 3.5 Å, whereas the region inside the micelle corresponding to the Sec61 was resolved between 3 and 7 Å **(Extended Data Figs. 3, 4)**. The EM density corresponding to the TRAP complex reveals its shape and relative orientation to the RNC as observed in low resolution cryo-EM and electron cryotomography (cryo-ET) maps[25–28]. The TRAP complex was resolved to around 6-8 Å resolution in the micelle area, showing a series of transmembrane alpha helices that allowed docking of a TRAPβγδ model predicted by AlphaFold2[29,30] **(Fig. 1b)**. Density corresponding to a single transmembrane helix (TMH) of TRAPα that according to the AlphaFold2 model stands separate from the other TRAP TMHs can also be observed (**Extended Data Fig. 5a)**. On the side of the ER lumen, the TRAP complex was resolved to around 8-12 Å, presenting a cradle-like density that extended towards the exit of the Sec61 pore. The shape of this entire volume was well described by a trimeric, β-sheet-containing TRAPαβδ model predicted by AlphaFold2 in multimer mode **(Fig. 1b)**. Additional confidence for correct docking came from the C-terminus of the TRAPα subunit, which was resolved at ~3.5 Å and unambiguously revealed the interactions with the ribosome at near-atomic detail **(Fig. 1c, Extended Data Figs. 3c, 4d)**. Inside the ribosomal exit tunnel, additional EM density representing the nascent chain is visible, however it disappears at the exit **(Extended Data Fig. 6)**. Therefore, in spite of the heterogeneous local resolution of the RNC-bound TRAP complex, combining the direct interpretation of better resolved regions of TRAP with AlphaFold2 predictions[31] for the regions where secondary structure elements were visible allowed us to generate a complete model of the RNC:Sec61:TRAP complex **(Fig. 1d, Extended Data Fig. 5)**.

bioRxiv preprint doi: https://doi.org/10.1101/2022.10.04.510795; this version posted October 4, 2022. The copyright holder for this preprint (which was not certified by peer review) is the author/funder, who has granted bioRxiv a license to display the preprint in perpetuity. It is made available under aCC-BY-NC-ND 4.0 International license.

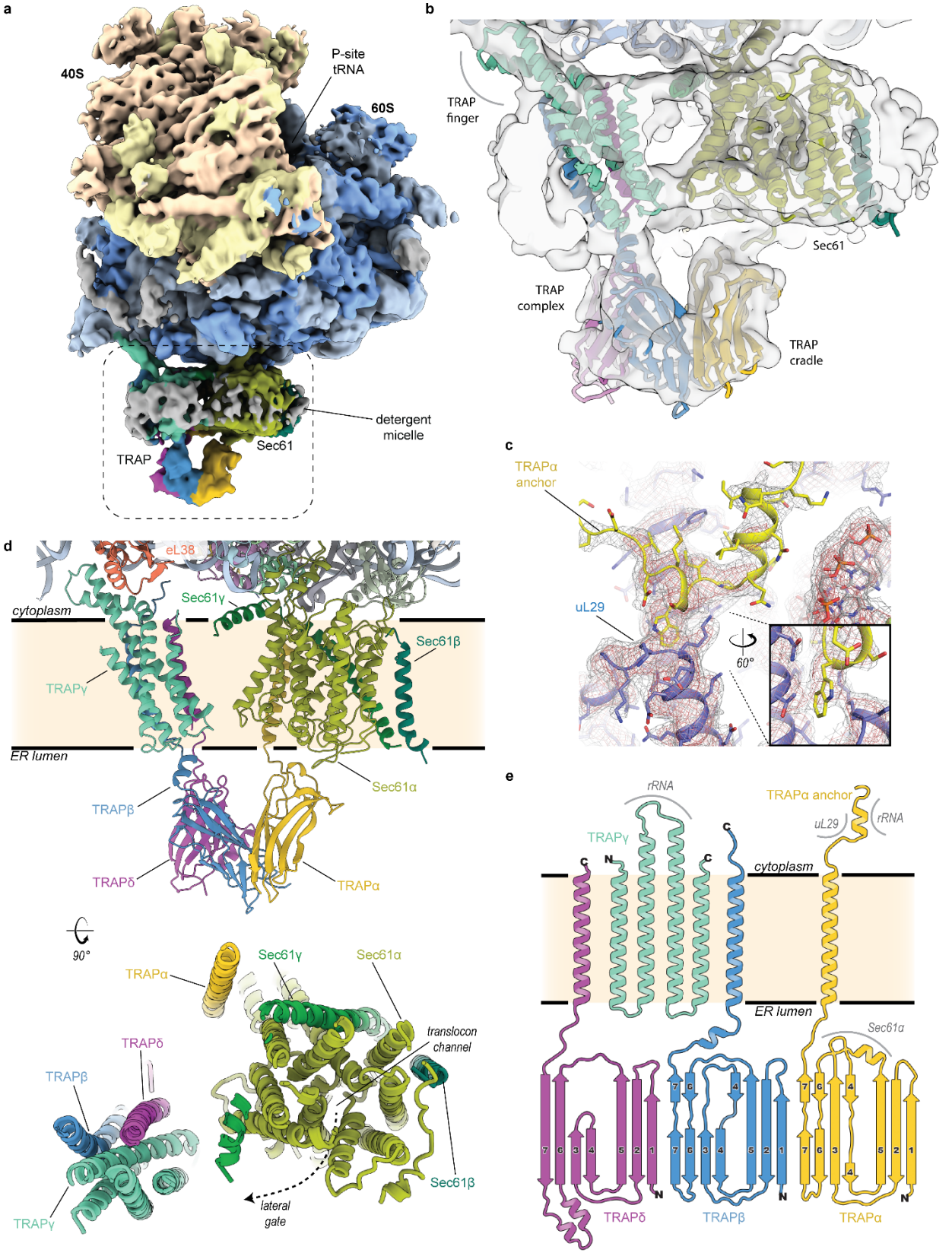

legend on the next page

bioRxiv preprint doi: https://doi.org/10.1101/2022.10.04.510795; this version posted October 4, 2022. The copyright holder for this preprint (which was not certified by peer review) is the author/funder, who has granted bioRxiv a license to display the preprint in perpetuity. It is made available under aCC-BY-NC-ND 4.0 International license.

Fig. 1 | Cryo-EM structure of the mammalian ribosome nascent chain complex (RNC), Sec translocon and TRAP ternary complex.

a, Cryo-EM map depicting TRAP, Sec translocon and the ribosome. Ribosomal proteins are colored brown and blue; the density of ribosomal RNA is colored yellow and light blue for the small and large subunit, respectively. Dashed box indicates the magnified region shown in (b). **b**, Cross section of the detergent micelle at the ribosomal exit tunnel. Densities and models of Sec translocon and TRAP complex are indicated. **c**, Closeup of the C-terminus of TRAPα (yellow) fitted into cryo-EM density shown as a mesh. Ribosomal protein uL29 (purple) is indicated. **d**, Closeup of the RNC:Sec61:TRAP atomic model. Sec translocon and TRAP complex proteins are labeled and colored individually. Ribosomal protein eL38 is shown. An overview of the Sec61:TRAP complex in the membrane as observed from the cytosolic side is shown below. Proteins are colored and labeled individually. The pore of the Sec translocon channel and the lateral gate are indicated. **e**, Secondary structure diagram of the TRAP complex. TRAP proteins are colored as in previous panels. N- and C-terminus of each protein is labeled. Regions that interact with the ribosome and the Sec translocon are indicated.

The TRAP complex is positioned near Sec61, but none of the TRAP TMHs are in direct contact with the translocon. The main bundle of TMHs formed by three TRAP subunits (TRAPβ, TRAPγ and TRAPδ) is positioned next to the lateral gate of Sec61, whereas the single TMH of TRAPα is located on the opposite side **(Fig. 1d)**. From the ER lumenal side, the immunoglobulin-like β-sandwich domains of TRAPα, TRAPβ and TRAPδ form a cradle-like domain that directly contacts the Sec translocon **(Fig. 1d,e)**.

TRAPα is anchored to the ribosome via its C-terminal tail

The prominent interaction between TRAP and the ribosome is mediated by the C-terminal tail of TRAPα folded in a hook-like shape that includes a short α-helix. These interactions occur in the vicinity of the exit of the ribosomal tunnel and involve insertion of a tryptophan between two helices of uL29 and electrostatic contacts with H9 of the 5.8S rRNA **(Fig. 2a, Extended Data Fig. 4d)**. Considering the specificity of these interactions it is likely that they contribute considerably to the affinity of the TRAP complex and that they are functionally important. Furthermore, alignment of TRAPα from different eukaryotic organisms, including plants and algae, shows a strong conservation of the anchor region including the tryptophan and a series of positively charged residues that point towards the negatively charged rRNA **(Fig. 2b)**. Consequently, we refer to this region as the TRAPα anchor. The location of the anchor, despite being in close proximity, neither overlaps with the SRP nor the Sec61 binding sites on the ribosome[11,21] (**Extended Data Fig. 7**). There is also no overlap with the recently observed ribosome contact areas of the nascent polypeptide-associated complex (NAC), an ER targeting regulator that recruits SRP to ribosomes[32] **(Extended Data Fig. 7).**

To validate the role of the anchor in TRAP function, we measured levels of a green fluorescent protein (GFP) reporter of ER stress driven by the hsp-4 promoter (hsp-4p::GFP) in *Caenorhabditis elegans*[33]. Consistent with a previous study[5], knockout of TRAPα in *C. elegans* resulted in a strong ER stress response, with elevated levels of the stress reporter hsp-4p::GFP detected throughout the worm body **(Fig. 2c)**, indicating a general function of the TRAP complex in maintaining ER protein homeostasis in cells.

bioRxiv preprint doi: https://doi.org/10.1101/2022.10.04.510795; this version posted October 4, 2022. The copyright holder for this preprint (which was not certified by peer review) is the author/funder, who has granted bioRxiv a license to display the preprint in perpetuity. It is made available under aCC-BY-NC-ND 4.0 International license.

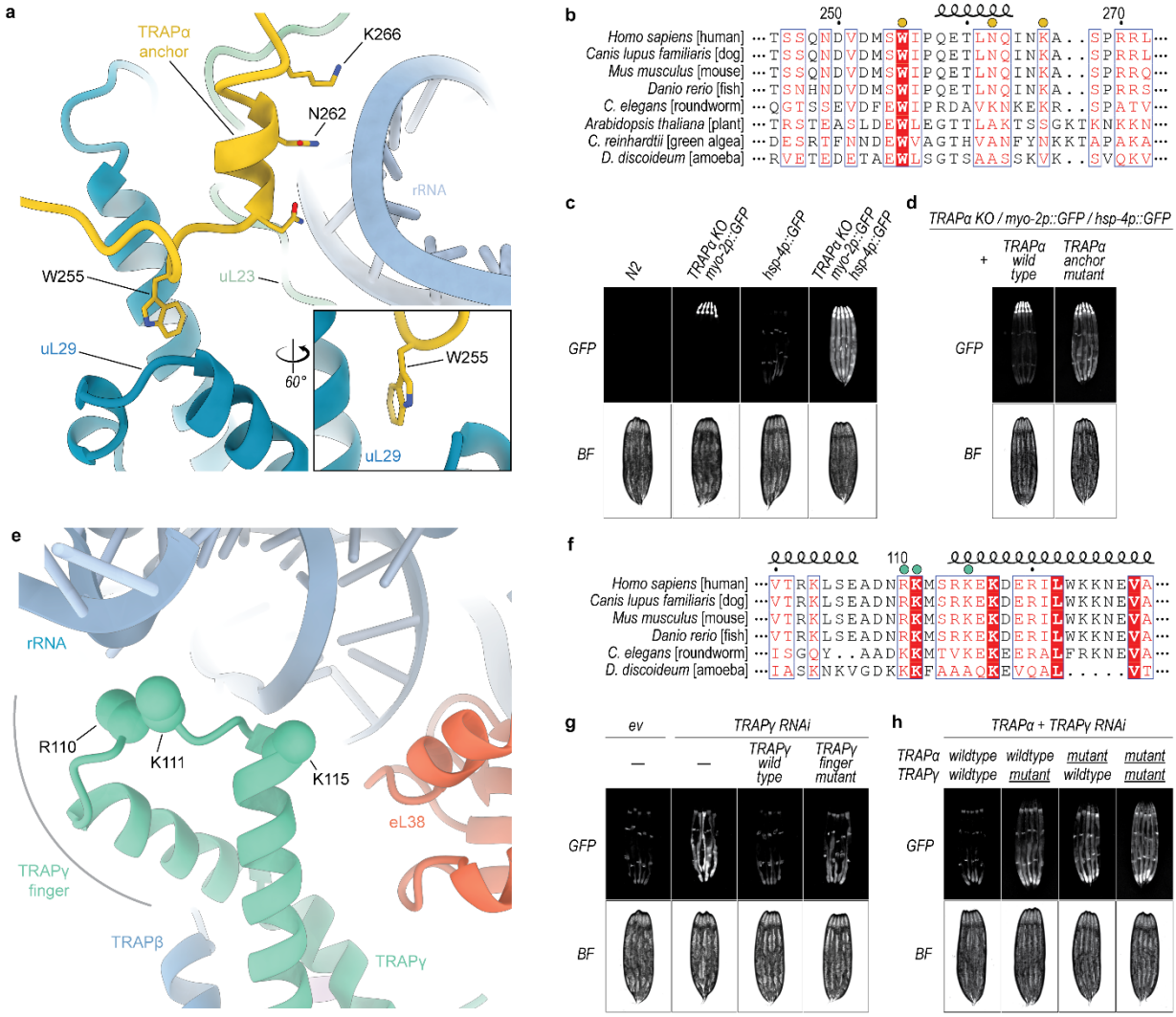

Fig. 2 | Molecular interactions of TRAP with the translating ribosome.

a, Atomic model of the TRAPα anchor. TRAPα (yellow) is shown in cartoon representation and the mutated residues that interact with ribosomal protein uL29 (blue) and ribosomal RNA (light blue) are indicated. **b**, Sequence alignment of TRAPα in eukaryotes. Mutated residues are indicated with a yellow dot above the sequence. **c**, Fluorescence microscope images of *C. elegans* TRAPα knockout (KO) strain carrying a pharynx-specific myo-2p::GFP expression cassette in the TRAPα gene locus, and the ER stress reporter hsp-4p::GFP. Wildtype N2 strain served as negative control. BF, bright field. **d**, Fluorescence microscope images of *C. elegans* TRAPα knockout (KO)/hsp-4p::GFP strain as in panel (c) complemented either with TRAPα wildtype or anchor mutant. **e**, Atomic model of the TRAPγ cytoplasmic domain. Positively charged residues of TRAPγ (green) that potentially interact with negatively charged ribosomal RNA (light blue) and were mutated are indicated. Ribosomal protein eL38 is shown in red. **f**, Sequence alignment of TRAPγ in eukaryotes. Mutated residues are indicated with a green dot above the sequence. **g**, Fluorescence microscope images of *C. elegans* expressing hsp-4p::GFP and carrying TRAPγ RNAi-resistant transgenes as indicated. Analysis was performed in the endogenous TRAPγ RNAi background on day 1 of adulthood. ev, empty vector RNAi control. BF, brightfield. **h**, Similar analysis as in panel (g), but in the endogenous TRAPα+γ RNAi background with strains expressing indicated RNAi-resistant TRAPα and TRAPγ transgenes.

bioRxiv preprint doi: https://doi.org/10.1101/2022.10.04.510795; this version posted October 4, 2022. The copyright holder for this preprint (which was not certified by peer review) is the author/funder, who has granted bioRxiv a license to display the preprint in perpetuity. It is made available under aCC-BY-NC-ND 4.0 International license.

We then designed a mutant of TRAPα that carries mutations in three residues (W228A, K235E and K239E, corresponding to human W255, N262 and K266, respectively) located within the anchor **(Fig. 2a,b)**. Worms expressing this mutant also showed increased levels of the ER stress reporter hsp-4p::GFP relative to the wild-type, especially in highly secretory intestinal cells **(Fig. 2d, Extended Data Fig. 8a)**, further highlighting the importance of this contact for TRAP function.

In addition to the TRAPα anchor, TRAP also interacts with the ribosome via less specific contacts between the negatively charged rRNA and a loop in the cytosolic domain of TRAPγ (referred to as the TRAPγ finger) harboring positively charged residues **(Fig. 2e)**, which are conserved in different eukaryotic organisms, as revealed by the sequence alignment of this region of the protein **(Fig. 2f)**. To better understand their importance, we designed a *C. elegans* mutant of TRAPγ that carries reverse charge mutations in three positively charged residues (R103E, K104E and K108E, corresponding to human R110, K111 and K115, respectively) **(Fig. 2e,f)**. Again, RNAi-mediated knockdown of TRAPγ in *C. elegans* caused significant ER stress, as indicated by increased levels of the ER stress reporter hsp-4p::GFP (**Fig. 2g).** While expression of wt-TRAPγ from an RNAi-resistant transgene completely reversed the observed ER stress phenotype, the TRAPγ finger mutant provided only partial rescue **(Fig. 2g, Extended Data Fig. 8b)**.

Considering that both the TRAPα anchor and the TRAPγ finger are important for TRAP interactions with the ribosome, we also investigated the levels of the ER stress reporter hsp-4p::GFP in *C. elegans* co-expressing the mutants of both proteins. As expected, ER stress was further enhanced in the double mutant worms, with the reporter hsp-4p::GFP now detected not only in the highly secretory intestinal cells but also in other tissues, such as muscle cells **(Fig. 2h, Extended Data Fig. 8c)**. In addition to ER stress, TRAPα knockout animals were significantly smaller **(Extended Data Fig. 8d)**, suggesting TRAP dysfunction causes a general growth defect in worms, consistent with the critical role of TRAP in the biosynthesis and secretion of insulin-like growth factors in *C. elegans*[5,34]. Animals expressing the mutant TRAP subunits, particularly the TRAPα anchor mutant, also exhibited a significant growth defect, suggesting that the ribosome contact of the TRAP complex is essential for proper cell growth and animal development **(Extended Data Fig. 8e)**.

These results suggest that the two ribosome contact points of TRAP have complementary roles. While the anchor provides affinity for TRAP, it is connected to the rest of TRAP via a long flexible linker and therefore does not restrain the position of TRAP relative to the ribosome or the translocon. In contrast, the cytosolic domain of TRAPγ contacts the ribosome via a finger-like loop flanked by α-helical elements, and therefore, together with the translocon contact of the lumenal domain of TRAPα (described below), helps in positioning the TRAP complex below the exit of the Sec61 channel.

bioRxiv preprint doi: https://doi.org/10.1101/2022.10.04.510795; this version posted October 4, 2022. The copyright holder for this preprint (which was not certified by peer review) is the author/funder, who has granted bioRxiv a license to display the preprint in perpetuity. It is made available under aCC-BY-NC-ND 4.0 International license.

The lumenal domain of TRAPα contacts the translocon and interacts with translocated proteins

Our structural results also show that TRAPα contacts the lumenal loop of Sec61α next to the protein-translocating pore. Based on the structure presented here, a highly conserved loop between beta sheets 5 and 6 of the lumenal domain of TRAPα **(Fig. 3a)** is in the position to interact with the loop between TMHs 5 and 6 of the Sec61α subunit of the translocon **(Fig. 3b,c)**. Mutation of the loop residues to polyserine (TRAPα loop mutant) in *C. elegans* significantly exacerbated the ER stress phenotype and growth defect of the TRAPα anchor mutant **(Fig. 3d, Extended Data Fig. 9)**. This suggests that the function of the TRAP complex relies on a dual binding mode of TRAPα interacting with both the translating ribosome in the cytosol and the translocating Sec61 pore in the ER lumen. Considering the positioning of TRAPα lumenal domain below the pore of the Sec translocon where it interacts with TRAPβ and TRAPδ to create a molecular cradle, it is reasonable to assume that it will interact with translocating nascent polypeptides. Analysis of the residues lining the surface of the cradle below the pore reveals the presence of numerous conserved aromatic and other hydrophobic residues in TRAPα, suggesting a possible role in interactions with the unfolded nascent polypeptides after passage through the translocon **(Fig. 3a-c)**. The observed molecular arrangement and the surface features of the complex are reminiscent of the mode of interaction between the bacterial trigger factor chaperone, which binds to the translating ribosome to present a hydrophobic cradle to the nascent chains of cytosolic proteins[35,36].

To test the importance of the conserved hydrophobic amino acids on the inside of the TRAP cradle **(Fig. 3a,e)**, we designed a mutant (TRAPα cradle mutant) in which these residues were mutated to threonine, a polar, uncharged amino acid. *C. elegans* worms expressing this mutant showed strongly increased expression levels of the ER stress reporter hsp-4p::GFP, especially in highly secretory intestinal cells **(Fig. 3f, Extended Data Fig. 9a)**. In addition, these worms also showed a pronounced growth defect similar in severity to the TRAPα anchor mutant **(Extended Data Fig. 9b)**. These results show that the cradle-shaped luminal domains of TRAP participate in the biogenesis of nascent chains as they are translocated into the ER lumen, possibly acting as a molecular chaperone. Similar domains exist in EMC, SPC22/23, OST, and Hsp70 and were proposed to have a chaperone-like function based on their structural features[36–39].

Previous studies suggested that TRAPα is essential for insulin secretion in human cells[5,6]. To investigate whether the ribosome-binding anchor and putative substrate-interacting cradle of TRAPα are important for insulin secretion, we used a genetic model of *C. elegans* insulin secretion carrying a mutation in the insulin receptor DAF-2/InsR that results in enhanced dauer larvae formation due to an insulin signaling defect[40,41]. Consistent with a previous study, knockout of TRAPα prevented dauer formation in DAF-2/InsR mutant animals, suggesting that secretion of insulin-like peptides in *C. elegans* depends on TRAP, similar to human cells[5] (**Fig. 3g**). While expression of wildtype TRAPα fully restored dauer

bioRxiv preprint doi: https://doi.org/10.1101/2022.10.04.510795; this version posted October 4, 2022. The copyright holder for this preprint (which was not certified by peer review) is the author/funder, who has granted bioRxiv a license to display the preprint in perpetuity. It is made available under aCC-BY-NC-ND 4.0 International license.

formation in TRAPα KO/DAF-2/InsR mutant animals, the TRAPα anchor and cradle mutant variants only showed minor activity, suggesting an insulin secretion defect in these animals (**Fig. 3g**).

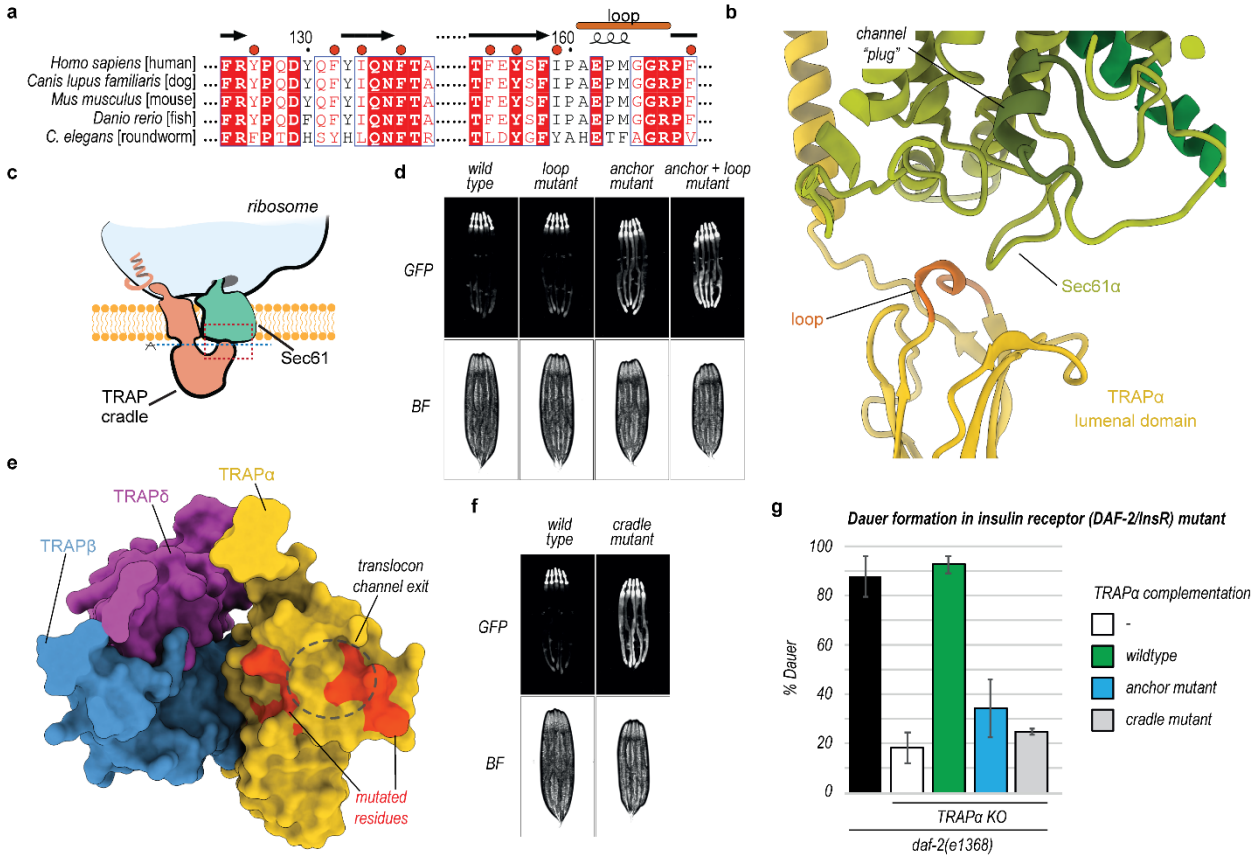

Fig. 3 | Molecular interactions between the lumenal side of TRAP and the Sec translocon.

a, Sequence alignment of TRAPα in eukaryotes. Loop that potentially contacts the Sec translocon are marked. Hydrophobic residues located within the cradle that were mutated are indicated with a red dot above the sequence. **b**, Closeup of the contact region between TRAP and the Sec translocon. Region of the closeup is marked with a dashed red box on a schematic in panel (c). Loop of TRAPα that potentially contacts Sec translocon is indicated and colored light brown. Translocon channel plug is labeled and shown in dark green. **c**, Schematic of the Sec translocon and TRAP complex bound to the ribosome. Dashed red box indicates the closeup region shown in panel (b). Dashed blue line indicates the plane of view used in panel (e). Ribosome, Sec translocon and TRAP cradle lumenal domain are labeled. **d**, Fluorescence microscope images of *C. elegans* TRAPα knockout worms expressing hsp-4p::GFP and indicated TRAPα variants. Analysis was performed on day 1 of adulthood. BF, brightfield. **e**, TRAP complex lumenal domain is shown as surface representation with proteins colored individually. Each TRAP protein that contributes to the lumenal domain is labeled. Sec translocon channel pore exit is indicated with a black dashed circle. Residues that were mutated are indicated in red. **f**, Fluorescence microscope images of *C. elegans* TRAPα knockout worms expressing hsp-4p::GFP and complemented with either wildtype TRAPα or the cradle mutant. **g**, TRAPα knockout worms expressing the indicated TRAPα variants and carrying the daf-2(e1368) mutation were grown at 24.5°C for 2 days. Diagram shows percentage of worms in the dauer state. Error bars, SD. n=3.

bioRxiv preprint doi: https://doi.org/10.1101/2022.10.04.510795; this version posted October 4, 2022. The copyright holder for this preprint (which was not certified by peer review) is the author/funder, who has granted bioRxiv a license to display the preprint in perpetuity. It is made available under aCC-BY-NC-ND 4.0 International license.

DISCUSSION

Based on the results presented here and previous insights into the structure and function of the TRAP complex[26,28], we propose a model for its participation in ER protein biogenesis (**Fig. 4a**). Initial interactions between ribosomes targeted to the ER and the TRAP complex occur via an evolutionarily conserved TRAPα anchor, which is flexibly tethered to the rest of TRAP. Considering that these contacts do not overlap with the position of SRP or NAC[21] **(Fig. 4b, Extended Data Fig. 7)** and that TRAP was observed to interact with nascent chains independent of the Sec translocon[6], it is possible that TRAP anchor contacts contribute to targeting of ribosomes to the ER. Once the ribosome binds the translocon, TRAP fully engages the ribosome stabilized by the additional electrostatic contacts with TRAPγ finger and interactions between the lumenal domain of TRAPα with the Sec61 translocon. In this conformation, a hydrophobic cradle formed of TRAPαβδ lumenal domains is positioned below the exit of the translocon pore for interactions with emerging nascent polypeptides. Our *in vivo* experiments in *C. elegans* show that the observed contacts and the hydrophobic character of the cradle, which possibly carry a chaperone-like functions, are critical for the biogenesis of secreted and membrane proteins in the ER.

Our results indicate that TRAPα fulfils two major functions of TRAP. It provides the anchor for the attachment to the ribosome as well as the hydrophobic domain that interacts with the Sec translocon and can aid in protein folding and biogenesis on the luminal side of the ER. It is therefore conceivable that the ancestral TRAP was a single domain protein that over the course of evolution acquired additional subunits, possibly in part through domain duplication as suggested by the similar domain folds of TRAPα, TRAPβ and TRAPδ **(Fig. 1d,e)**, which helped stabilize the complex and optimize its positioning next to the exit of the translocon pore. This hypothesis is supported by the observation that a reduced functional TRAP complex, composed of only TRAPα and TRAPβ, exists in plants and algae[26]. This system would be able to fulfill all key roles of TRAP[42], however, compared to the tetrameric mammalian TRAP, it would lack the additional stabilizing electrostatic interactions mediated by TRAPγ.

Considering its position relative to the RNC and the Sec translocon, it is likely that TRAP can act on nascent chains simultaneously with several other protein complexes known to participate in protein translocation, such as OST[24] or the factors involved in the formation of multi-pass membrane proteins, such as PAT complex or TMCO1 translocon[43,44]. However, it is also likely that TRAP may need to occasionally move in or out of its position next to the translocon to allow sequential access of a range of other nascent chain interacting factors in the ER, such as TRAM (translocating chain-associating membrane protein), signal peptidase complexes and EMC (endoplasmic reticulum membrane protein complex)[9,13]. Our results explain how TRAP would be able to accomplish this task through flexible anchor attachment. A similar mode of action has recently been observed for NAC, as it tethers SRP to control its access to the signal sequence-containing nascent chains[32]. The structural and *in vivo* results presented in this manuscript reveal

bioRxiv preprint doi: https://doi.org/10.1101/2022.10.04.510795; this version posted October 4, 2022. The copyright holder for this preprint (which was not certified by peer review) is the author/funder, who has granted bioRxiv a license to display the preprint in perpetuity. It is made available under aCC-BY-NC-ND 4.0 International license.

the molecular basis of TRAP participation in the biogenesis and translocation of proteins in the ER and pave the way for future structure-based experiments.

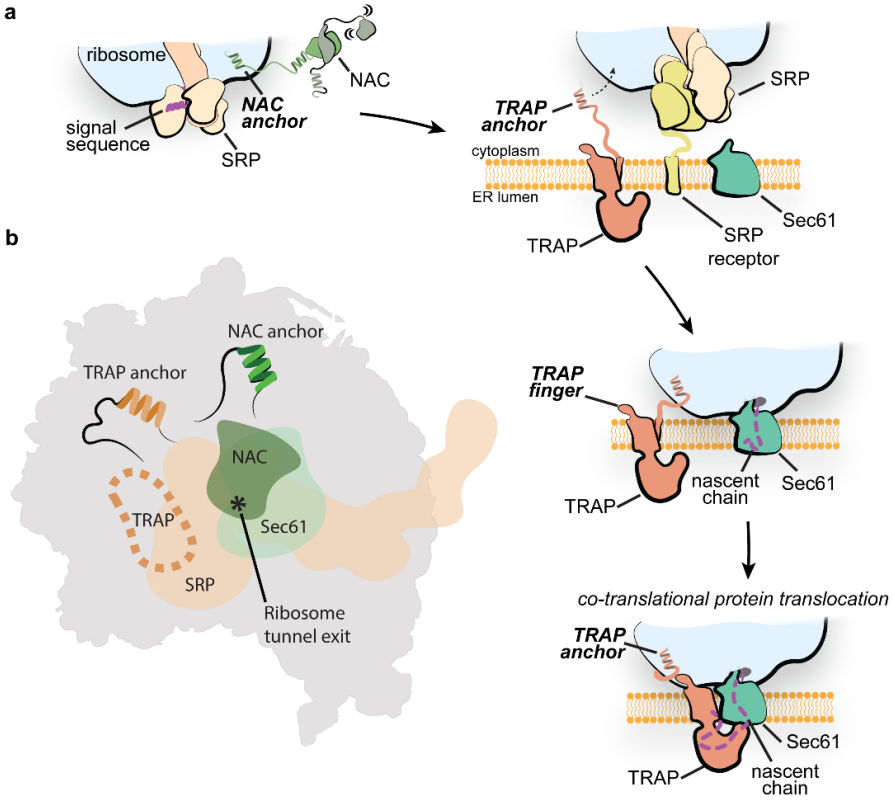

Fig. 4 | Model of TRAP function in protein translocation across the ER membrane.

a, Schematic of the proposed function of the TRAP complex. The interplay of NAC and SRP initiates the targeting of the translating ribosome carrying an ER client to the ER membrane. Interaction with the SRP receptor at the ER membrane then initiates the transfer of the ribosome to Sec translocon. The tethered ribosome interacting TRAPα anchor could facilitate the transfer by attaching the ribosome near the Sec translocon. Once the handover has occurred, the TRAP-RNC-Sec61 complex is additionally stabilized by the TRAPγ finger on the ribosome as well as the TRAPα lumenal loop interacting with the translocon. In this conformation, the TRAP complex positions a hydrophobic cradle-like lumenal domain directly at the exit of the Sec61 pore, which could act as a chaperone for the incoming nascent chain. **b**, Schematic depicting the binding sites of SRP, NAC, and Sec translocon on the ribosome exit tunnel region. The binding site of the TRAP anchor and NAC anchor are indicated. Binding site of TRAP finger is indicated with a dashed line. The position of the ribosome polypeptide tunnel exit is indicated with an asterisk.

bioRxiv preprint doi: https://doi.org/10.1101/2022.10.04.510795; this version posted October 4, 2022. The copyright holder for this preprint (which was not certified by peer review) is the author/funder, who has granted bioRxiv a license to display the preprint in perpetuity. It is made available under aCC-BY-NC-ND 4.0 International license.

REFERENCES

1. Matlack, K. E. S. & Walter, P. The 70 Carboxyl-terminal Amino Acids of Nascent Secretory Proteins Are Protected from Proteolysis by the Ribosome and the Protein Translocation Apparatus of the Endoplasmic Reticulum Membrane. *J. Biol. Chem.* **270**, 6170–6180 (1995).
2. Görlich, D., Prehn, S., Hartmann, E., Kalies, K. U. & Rapoport, T. A. A mammalian homolog of SEC61p and SECYp is associated with ribosomes and nascent polypeptides during translocation. *Cell* **71**, 489–503 (1992).
3. Fons, R. D., Bogert, B. A. & Hegde, R. S. Substrate-specific function of the translocon-associated protein complex during translocation across the ER membrane. *J. Cell Biol.* **160**, 529–539 (2003).
4. Hartmann, E. *et al.* A tetrameric complex of membrane proteins in the endoplasmic reticulum. *Eur. J. Biochem.* **214**, 375–81 (1993).
5. Li, X. *et al.* Requirement for translocon-associated protein (TRAP) α in insulin biogenesis. *Sci. Adv.* **5**, (2019).
6. Kriegler, T., Kiburg, G. & Hessa, T. Translocon-Associated Protein Complex (TRAP) is Crucial for Co-Translational Translocation of Pre-Proinsulin. *J. Mol. Biol.* **432**, 166694 (2020).
7. Uhlén, M. *et al.* Tissue-based map of the human proteome. *Science* **347**, (2015).
8. Nyathi, Y., Wilkinson, B. M. & Pool, M. R. Co-translational targeting and translocation of proteins to the endoplasmic reticulum. *Biochim. Biophys. Acta - Mol. Cell Res.* **1833**, 2392–2402 (2013).
9. Hegde, R. S. & Keenan, R. J. The mechanisms of integral membrane protein biogenesis. *Nat. Rev. Mol. Cell Biol.* **23**, 107–124 (2022).
10. Rapoport, T. A., Li, L. & Park, E. Structural and Mechanistic Insights into Protein Translocation. *Annu. Rev. Cell Dev. Biol.* **33**, 369–390 (2017).
11. Voorhees, R. M. & Hegde, R. S. Structure of the Sec61 channel opened by a signal sequence. *Science* **351**, 88–89 (2016).
12. Zimmer, J., Nam, Y. & Rapoport, T. A. Structure of a complex of the ATPase SecA and the protein-translocation channel. *Nature* **455**, 936–943 (2008).
13. Liaci, A. M. & Förster, F. Take Me Home, Protein Roads: Structural Insights into Signal Peptide Interactions during ER Translocation. *Int. J. Mol. Sci. 2021, Vol. 22, Page 11871* **22**, 11871 (2021).
14. Nguyen, D. *et al.* Proteomics reveals signal peptide features determining the client specificity in human TRAP-dependent ER protein import. **9**, 1–15 (2018).
15. Webb, G. C., Akbar, M. S., Zhao, C. & Steiner, D. F. Expression profiling of pancreatic β cells: Glucose regulation of secretory and metabolic pathway genes. *Proc. Natl. Acad. Sci. U. S. A.* **97**, 5773–5778 (2000).
16. Mahajan, A. *et al.* Genome-wide trans-ancestry meta-analysis provides insight into the genetic architecture of type 2 diabetes susceptibility. *Nat. Genet. 2014 463* **46**, 234–244 (2014).
17. Mesbah, K., Camus, A., Babinet, C. & Barra, J. Mutation in the Trapalpha/Ssr1 gene, encoding translocon-associated protein alpha, results in outflow tract morphogenetic defects. *Mol. Cell. Biol.* **26**, 7760–71 (2006).
18. Losfeld, M. E. *et al.* A new congenital disorder of glycosylation caused by a mutation in SSR4, the signal sequence receptor 4 protein of the TRAP complex. *Hum. Mol. Genet.* **23**, 1602–1605 (2013).
19. Li, D. H. *et al.* The role of XTRAP-gamma in Xenopus pronephros development. *Int. J. Dev. Biol.* **49**, 401–408 (2004).
20. Yamaguchi, Y. L. *et al.* Translocon-associated protein subunit Trap-γ/Ssr3 is required for vascular network formation in the mouse placenta. *Dev. Dyn.* **240**, 394–403 (2011).
21. Jomaa, A. *et al.* Molecular mechanism of cargo recognition and handover by the mammalian signal recognition particle. *Cell Rep.* **36**, 109350 (2021).
22. Walter, P. & Blobel, G. Preparation of microsomal membranes for cotranslational protein translocation. *Methods Enzymol.* **96**, 84–93 (1983).
23. Ramírez, A. S., Kowal, J. & Locher, K. P. Cryo-electron microscopy structures of human oligosaccharyltransferase complexes OST-A and OST-B. *Science* **366**, (2019).
24. Braunger, K. *et al.* Structural basis for coupling protein transport and N-glycosylation at the

bioRxiv preprint doi: https://doi.org/10.1101/2022.10.04.510795; this version posted October 4, 2022. The copyright holder for this preprint (which was not certified by peer review) is the author/funder, who has granted bioRxiv a license to display the preprint in perpetuity. It is made available under aCC-BY-NC-ND 4.0 International license.

mammalian endoplasmic reticulum. *Science* **360**, 215–219 (2018).
25. Voorhees, R. M., Fernández, I. S., Scheres, S. H. W. & Hegde, R. S. Structure of the Mammalian Ribosome-Sec61 Complex to 3.4 Å Resolution. *Cell* **157**, 1632–1643 (2014).
26. Pfeffer, S. *et al.* Dissecting the molecular organization of the translocon-associated protein complex. *Nat. Commun.* **8**, 14516 (2017).
27. Pfeffer, S. *et al.* Structure of the native Sec61 protein-conducting channel. *Nat. Commun.* **6**, (2015).
28. Ménétret, J.-F. *et al.* Single Copies of Sec61 and TRAP Associate with a Nontranslating Mammalian Ribosome. *Structure* **16**, 1126–1137 (2008).
29. Jumper, J. *et al.* Highly accurate protein structure prediction with AlphaFold. *Nature* **596**, (2021).
30. Evans, R. *et al.* Protein complex prediction with AlphaFold-Multimer. *bioRxiv* 2021.10.04.463034 (2022) doi:10.1101/2021.10.04.463034.
31. Mirdita, M. *et al.* ColabFold: making protein folding accessible to all. *Nat. Methods 2022 196* **19**, 679–682 (2022).
32. Jomaa, A. *et al.* Mechanism of signal sequence handover from NAC to SRP on ribosomes during ER-protein targeting. *Science* **375**, 839–844 (2022).
33. Calfon, M. *et al.* IRE1 couples endoplasmic reticulum load to secretory capacity by processing the XBP-1 mRNA. *Nature* **415**, (2002).
34. Murphy, C. T. & Hu, P. J. Insulin/insulin-like growth factor signaling in C. elegans. *WormBook : the online review of C. elegans biology* (2013) doi:10.1895/wormbook.1.164.1.
35. Kramer, G., Boehringer, D., Ban, N. & Bukau, B. The ribosome as a platform for co-translational processing, folding and targeting of newly synthesized proteins. *Nat. Struct. Mol. Biol. 2009 166* **16**, 589–597 (2009).
36. Pleiner, T. *et al.* Structural basis for membrane insertion by the human ER membrane protein complex. *Science* **369**, 433–436 (2020).
37. Mayer, M. P. & Bukau, B. Hsp70 chaperones: Cellular functions and molecular mechanism. *Cell. Mol. Life Sci.* **62**, 670 (2005).
38. Wild, R. *et al.* Structure of the yeast oligosaccharyltransferase complex gives insight into eukaryotic N-glycosylation. *Science* **359**, 545–550 (2018).
39. Liaci, A. M. *et al.* Structure of the human signal peptidase complex reveals the determinants for signal peptide cleavage. *Mol. Cell* **81**, 3934-3948.e11 (2021).
40. Kimura, K. D., Tissenbaum, H. A., Liu, Y. & Ruvkun, G. daf-2, an insulin receptor-like gene that regulates longevity and diapause in Caenorhabditis elegans. *Science* **277**, 942–946 (1997).
41. Fielenbach, N. & Antebi, A. C. elegans dauer formation and the molecular basis of plasticity. *Genes Dev.* **22**, 2149–2165 (2008).
42. Phoomak, C. *et al.* The translocon-associated protein (TRAP) complex regulates quality control of N-linked glycosylation during ER stress. *Sci. Adv.* **7**, (2021).
43. Chitwood, P. J. & Hegde, R. S. An intramembrane chaperone complex facilitates membrane protein biogenesis. *Nat. 2020 5847822* **584**, 630–634 (2020).
44. McGilvray, P. T. *et al.* An ER translocon for multi-pass membrane protein biogenesis. *Elife* **9**, 1–43 (2020).

bioRxiv preprint doi: https://doi.org/10.1101/2022.10.04.510795; this version posted October 4, 2022. The copyright holder for this preprint (which was not certified by peer review) is the author/funder, who has granted bioRxiv a license to display the preprint in perpetuity. It is made available under aCC-BY-NC-ND 4.0 International license.

METHODS

Preparation of mammalian ribosome nascent chain complex

The ribosome nascent chain complex was prepared and purified as previously described[21]. Briefly, a plasmid encoding 3xFLAG-tag followed by an N-terminal fragment of the yeast dipeptidyl aminopeptidase B protein (24-90 amino acids)[45] was linearized using PstI restriction enzyme and used for mRNA generation in in vitro transcription with the T7 RNA polymerase. The mRNA at a concentration of 214 ng/µL was translated in the Flexi Rabbit Reticulocyte Lysate System (Promega) for 25 minutes at 32°C resulting in run-off ribosome nascent chain complex (RNC). The RNCs were purified using FLAG-tag affinity chromatography. Approximately 0.5 mL of ANTI-FLAG M2 Affinity Gel (SIGMA-ALDRICH) was washed with buffer A (50 mM HEPES-KOH pH 7.6, 100 mM KCl, 5 mM $MgCl_2$) and incubated with 4.7 mL of the translation reaction product for 2 hours at 4°C in chromatography column. The supernatant was then removed by gravity flow and the gel was washed by 10 mL of buffer B (50 mM HEPES-KOH pH 7.6, 500 mM KCl, 5 mM $MgCl_2$) and 10 mL of buffer A (50 mM HEPES-KOH pH 7.6, 100 mM KCl, 5 mM $MgCl_2$). The RNCs were eluted in 3 fractions (1 mL each) with buffer A containing 0.1 mg/mL 3xFLAG Peptide. All fractions were pooled and the RNCs were pelleted by ultracentrifugation in a TLA55 rotor (Beckman Coulter) at 50000 rpm and 4°C for 2 hours. Finally, the RNC pellet was resuspended in buffer C (50 mM HEPES-KOH pH 7.6, 100 mM KOAc, 5 mM $Mg(OAc)_2$) to a final concentration of 360 nM. The sample was flash-frozen in liquid nitrogen and stored at -80°C.

Cryo-EM sample preparation

The mammalian RNCs were incubated with canine SRP (tRNA Probes LLC) at a final concentration of 100 nM RNC and 140 nM SRP in a buffer R1 (50 mM HEPES-KOH pH 7.4, 5 mM $MgCl_2$, 150 mM KOAc, 300 mM sucrose, 5 mM Guanosine-5'-[(β,γ)-imido]triphosphate (GNP) for 10 minutes at 30°C. Concurrently, 20 µL of EKRM (tRNA Probes LLC) were incubated for 5 minutes on ice in buffer R2 (50 mM HEPES-KOH pH 7.4, 5 mM $MgCl_2$, 150 mM KOAc, 440 mM sucrose, 5 mM GNP, 1 mM RNaseOUT). Afterwards, both reactions were mixed together and incubated for 10 minutes at 30°C. The EKRM were then solubilized with 2% digitonin for 15 minutes at 4°C and the reaction was then spun down for 10 minutes at 12000 xg and 4°C. The supernatant was carefully layered onto a 100 µL of buffer C (50 mM HEPES-KOH pH 7.4, 5 mM $MgCl_2$, 150 mM KOAc, 0.025% GDN, 1.4 M sucrose) and the sucrose cushion was ultra-centrifuged for 1.5 hours at 80000 rpm and 4°C in TLA-100 rotor (Beckman Coulter). The pellet was resuspended in 100 µL of buffer F (50 mM HEPES-KOH pH 7.4, 5 mM $MgCl_2$, 150 mM KOAc, 0.025% GDN, glyco-diosgenin) and spun down again for 10 minutes at 12000 rcf and 4°C. The final sample in the supernatant was transferred into a fresh tube and use immediately for cryo-EM grids preparation.

Cryo-EM grids preparation and data collection

The Quantifoil R2/2 holey carbon grids were washed with ethyl acetate, coated with an extra layer of carbon and glow discharged with 15 mA for 15 seconds in Pelco EasyGlow system. Each grid was mounted onto the ThermoFisher Vitrobot IV and 3.5 µL of sample was incubated on the grid for 60 seconds at 4°C and 100% humidity before being blotted and plunged into liquid ethane/propane mix cooled to liquid nitrogen temperature. Several grids with different blotting times were prepared from the sample at approximate 400 nM, 200 nM and 100 nM ribosome concentration (based on absorbance at 260 nm wavelength).
Data was collected on Titan Krios electron microscope operated at 300 kV and equipped with the Gatan K3 direct electron detector and Gatan Imaging Filter with an energy filter slot width of 20 eV. Automated data acquisition in counting mode was performed using EPU software. Data was collected at a nominal magnification of 81000x and a defocus range of -1.2 to -3 µm, with a pixel size of 1.06 Å/pixel. Micrographs were recorded as movie stacks with an electron dose of ~60 electrons/$Å^2$.

bioRxiv preprint doi: https://doi.org/10.1101/2022.10.04.510795; this version posted October 4, 2022. The copyright holder for this preprint (which was not certified by peer review) is the author/funder, who has granted bioRxiv a license to display the preprint in perpetuity. It is made available under aCC-BY-NC-ND 4.0 International license.

Cryo-EM data processing

A total of 4 datasets were collected from two different cryo-EM grid preparations. Two data collections, dataset 1.1 and dataset 1.2, containing 9,373 and 25,548 movies, respectively, were collected from the same grid preparation. These two datasets were then merged into dataset 1 and imported into RELION 3.1[46] with separate optics groups. Dataset 2 was composed of dataset 2.1 (6,628 movies) and dataset 2.2 (23,235 movies) prepared from the second grid preparation. Both datasets were motion corrected with MotionCorr2[47] and the micrographs CTF was estimated using CTFFind4[48]. Particles were picked in RELION using 80S ribosome as a reference. Extracted particles (binned, at a pixel size of 6.784 Å) were subjected to 2D image classification. Particles from 2D class averages that depict well-resolved ribosomes were picked from both datasets, merged together and subjected to another round of 2D classification. Classified particles were selected into one of 3 groups according to their class averages: ribosome particles, ribosome-like particles and protein-like particles. Each group was subjected to three rounds of 3D classification with an 80S ribosome as a reference lowpass filtered to 60 Å resolution. Selected 610,191 ribosomal particles were re-extracted with a 1.428 Å/pix and a box of 320x320 pixels and were 3D auto-refined using lowpass filtered 80S ribosome as a reference, with per-particle CTF and aberration correction. Focused 3D classification was then performed with a mask surrounding the exit tunnel of the ribosome and the micelle region. This was used to improve the density for the TRAP and Sec translocon complexes. Classification was performed without particle alignments as described in RELION [46], with regularization parameter T=3 and limiting the resolution in the E-step to 5 Å. The class showing a strong density for the detergent micelle and an extra lumenal domain of TRAP and Sec translocon was selected. A second round of focused 3D classification to further improve the occupancy of the TRAP complex. A class composed of 114,154 particles with a strong density of the Sec translocon was selected and 3D auto refined. A final round of focused 3D classification was performed using a mask surrounding the TRAP complex only, with a regularization parameter T=10, E-step limit resolution of 6 Å. The class depicting the best resolved density for the TRAP complex was selected containing 22,643 particles, re-extracted without rescaling (pixel size of 1.06 Å) and was then 3D refined to a global resolution of 3.5 Å.

Model building

A recently published high resolution model of the rabbit 80S ribosome (PDB 7O7Y)[49] was docked into the cryo-EM map using UCSF ChimeraX[50] and readjusted manually in COOT[51]. This included repositioning of the large subunit stalks as well as residues lining the nascent chain tunnel and the tunnel exit, where the ribosome contacts the Sec61 translocon. Coordinates for the Sec61 translocon were used based on the PDB 6W6L[44] and rebuilt in the areas where the map reached near-atomic resolution **(Extended Data Fig. 4)**. For building of a P-site acyl-tRNA (His) template together the attached nascent chain, a recently published high-resolution cryo-EM map of the same ribosome nascent chain complex (EMD-12801) served as a guide, and the resulting model was transplanted into the current map. The sequence for the tRNA (tRNA-His-GTG-1-1) was obtained from the GtRNAdb database[52]. An initial molecular model of the tetrameric TRAP complex was predicted with AlphaFold2 in multimer mode[30,31]. The model was docked into the cryo-EM map using UCSF ChimeraX, and discrete parts (the lumenal domains of TRAPαβδ, the transmembrane domain bundle comprising TRAP and the transmembrane helix of TRAPα) were readjusted by rigid body fitting in COOT. The high quality of the EM-map corresponding to the C-terminal TRAPα anchor allowed unambiguous sequence assignment and *de-novo* building **(Fig. 1c)**.

The assembled model was subjected to five cycles of real space refinement using PHENIX version 1.20.1[53] including side chain rotamer and Ramachandran restraints **(Extended Data Table S1)**. The model geometry was validated using MolProbity[54]. The refined model shows an excellent geometry and map correlation, and the resolution of the model vs. map FSC at a value of 0.5 coincides well with the one determined between the map half-sets at a FSC=0.143 criterion **(Extended Data Table S1)**.

bioRxiv preprint doi: https://doi.org/10.1101/2022.10.04.510795; this version posted October 4, 2022. The copyright holder for this preprint (which was not certified by peer review) is the author/funder, who has granted bioRxiv a license to display the preprint in perpetuity. It is made available under aCC-BY-NC-ND 4.0 International license.

In vivo experiments

C. elegans strains and transformation

C. elegans worms were cultured according to standard techniques with *E. coli* OP50 as food source[55]. ER stress reporter strain SJ4005 (zcIs4[hsp-4p::GFP])[33], TRAPα knock-out strain VC4892, in which the TRAPα gene is replaced by a selection cassette (gk5960[loxP + myo-2p::GFP::unc-54 3'UTR + rps-27p::neoR::unc-54 3'UTR + loxP])[56], and insulin receptor mutant strain DR1572 (daf-2(e1368) III.) were obtained from the Caenorhabditis Genetics Center (CGC, University of Minnesota, USA). Wildtype Bristol N2 strain was used for all transformations. Transgenic strains were generated using standard microinjection protocols [57]. Transgene integration was performed using the miniMos transposon method[58]. Strains carrying RNAi-resistant genes of TRAPα and TRAPγ were constructed as previously described[59]. In brief, RNAi-resistant coding sequences of *C. elegans* TRAPα (*trap-1*) and TRAPγ (*trap-3*) were designed using a codon adaptation tool[60] and synthesized by Integrated DNA Technologies, Inc. (IDT). The coding sequences including three synthetic introns and a C-terminal FLAG tag are listed in **Extended Data Table S2 and S3**. The genes were subcloned into miniMos pCFJ910 vector (Addgene plasmid #44481)[58] under control of the endogenous *trap-1* and *trap-3* promoter regions and 3'UTRs. A separate fluorescent marker gene (mCherry) was added to the constructs to identify knock-in animals. Detailed strain information is available in **Extended Data Table S4**.

ER stress reporter analysis

Worm strains carrying RNAi-resistant TRAP genes were mated to the ER stress reporter strain SJ4005 expressing GFP under control of the ER stress-inducible *hsp-4* promoter (hsp-4p::GFP)[33]. Single and double RNAi constructs targeting endogenous *trap-1* and *trap-3* were cloned by inserting the spliced coding sequences of *trap-1* and *trap-3* into vector L4440 (Addgene plasmid #1654). The constructs were then transformed into the RNAi feeding *E. coli* strain HT115 [61]. Endogenous TRAP genes were silenced in worms from hatch on plates containing the respective HT115 RNAi bacteria. Worms were grown on RNAi plates at 20°C until adulthood. Adult animals were then immobilized with 1% sodium azide and GFP fluorescence was assessed using a DM6000B-Cs microscope (Leica) equipped with a DFC 365FX camera (Leica) and a 5x objective. Strains carrying TRAPα genes and hsp-4p::GFP were additionally analyzed in the TRAPα knock-out background without performing RNAi by crossing with the TRAPα knock-out strain VC4892, in which GFP is constitutively expressed in the pharynx (myo-2p::GFP). ER stress was assessed similarly in adult worms grown at 20°C but with *E. coli* OP50 as food source.

Worm growth analysis

Strains carrying RNAi-resistant TRAPα and TRAPγ genes were grown on RNAi plates from hatch until adulthood at 20°C to silence expression of the endogenous TRAP genes. 20 gravid adult worms of each strain were then allowed to lay eggs on a fresh RNAi plate for 4 hours. Adult worms were removed, and plates kept at 25°C. The development of the worms was analyzed after 24, 48 and 72 hours by determining the axial length of the worms (time-of-flight, TOF) by worm flow cytometry using a COPAS FlowPilot (Union Biometrica).

Dauer arrest assay

Dauer arrest assays were performed with C. elegans strain DR1572 (daf-2(e1368) III) as previously described[5]. In brief, gravid hermaphrodites were transferred to a fresh assay plate for synchronized egg lay at 20°C. Adult animals were removed, and plates were transferred to 24.5°C and scored for dauers after 2 days. The experiment was performed three times.

Immunoblotting and antibodies

Expression levels of the TRAP knock-in genes were analyzed by detection of the C-terminal FLAG tag using standard immunoblotting techniques as described previously[62]. Following commercial antibodies were used: FLAG (Sigma, #F7425), GAPDH (Santa Cruz, #sc-137179). Tubulin antibodies were a kind gift of Thomas Mayer, University of Konstanz.

bioRxiv preprint doi: https://doi.org/10.1101/2022.10.04.510795; this version posted October 4, 2022. The copyright holder for this preprint (which was not certified by peer review) is the author/funder, who has granted bioRxiv a license to display the preprint in perpetuity. It is made available under aCC-BY-NC-ND 4.0 International license.

METHODS REFERENCES

45. Kobayashi, K. *et al.* Structure of a prehandover mammalian ribosomal SRP·SRP receptor targeting complex. *Science* **360**, 323–327 (2018).
46. Zivanov, J. *et al.* New tools for automated high-resolution cryo-EM structure determination in RELION-3. *Elife* **7**, (2018).
47. Zheng, S. Q. *et al.* MotionCor2: anisotropic correction of beam-induced motion for improved cryo-electron microscopy. *Nat. Methods* **14**, 331–332 (2017).
48. Rohou, A. & Grigorieff, N. CTFFIND4: Fast and accurate defocus estimation from electron micrographs. *J. Struct. Biol.* **192**, (2015).
49. Bhatt, P. R. *et al.* Structural basis of ribosomal frameshifting during translation of the SARS-CoV-2 RNA genome. *Science* **372**, (2021).
50. Goddard, T. D. *et al.* UCSF ChimeraX: Meeting modern challenges in visualization and analysis. *Protein Sci.* **27**, 14–25 (2018).
51. Emsley, P., Lohkamp, B., Scott, W. G. & Cowtan, K. Features and development of Coot. *Acta Crystallogr. Sect. D Biol. Crystallogr.* **66**, 486–501 (2010).
52. Lowe, T. M. & Chan, P. P. tRNAscan-SE On-line: integrating search and context for analysis of transfer RNA genes. *Nucleic Acids Res.* **44**, W54–W57 (2016).
53. Adams, P. D. *et al.* PHENIX: A comprehensive Python-based system for macromolecular structure solution. *Acta Crystallogr. Sect. D Biol. Crystallogr.* **66**, (2010).
54. Williams, C. J. *et al.* MolProbity: More and better reference data for improved all-atom structure validation. *Protein Sci.* **27**, 293–315 (2018).
55. Brenner, S. The genetics of Caenorhabditis elegans. *Genetics* **77**, (1974).
56. Au, V. *et al.* CRISPR/Cas9 methodology for the generation of knockout deletions in caenorhabditis elegans. *G3 Genes, Genomes, Genet.* **9**, (2019).
57. Mello, C. & Fire, A. Chapter 19 DNA Transformation. in (1995). doi:10.1016/s0091-679x(08)61399-0.
58. Frøkjær-Jensen, C. *et al.* Random and targeted transgene insertion in Caenorhabditis elegans using a modified Mos1 transposon. *Nat. Methods* **11**, (2014).
59. Gamerdinger, M. *et al.* Early Scanning of Nascent Polypeptides inside the Ribosomal Tunnel by NAC. *Mol. Cell* **75**, (2019).
60. Redemann, S. *et al.* Codon adaptation-based control of protein expression in C. elegans. *Nat. Methods* **8**, (2011).
61. Timmons, L., Court, D. L. & Fire, A. Ingestion of bacterially expressed dsRNAs can produce specific and potent genetic interference in Caenorhabditis elegans. *Gene* **263**, (2001).
62. Gamerdinger, M., Hanebuth, M. A., Frickey, T. & Deuerling, E. The principle of antagonism ensures protein targeting specificity at the endoplasmic reticulum. *Science* **348**, 201–207 (2015).

bioRxiv preprint doi: https://doi.org/10.1101/2022.10.04.510795; this version posted October 4, 2022. The copyright holder for this preprint (which was not certified by peer review) is the author/funder, who has granted bioRxiv a license to display the preprint in perpetuity. It is made available under aCC-BY-NC-ND 4.0 International license.

Data Availability Statement

The data supporting the findings of this study are available in the Electron Microscopy and Protein Data Bank under accession codes EMD-XXXX and PDB ID - XXXX.

Materials & Correspondence

Correspondence and requests for materials should be addressed to Ahmad Jomaa, Elke Deuerling and Nenad Ban.

Acknowledgements

We thank members of the Ban and Deuerling labs for discussions. We thank A. Scaiola for help with EM data collection. We thank R. Schloemer and G. Hunaeus for technical assistance. Cryo-EM was collected at ScopeM at the ETH Zurich. This manuscript is dedicated to Saša Ban.

Author Contributions

A.J., M.J. and N.B. conceived the study. M.J., A.J., M.G., E.D. and N.B. designed the experiments and analyzed the results. A.J. and M.J. prepared ribosome nascent chain complexes, assembled the ER-bound complex, and prepared samples for cryo-EM experiments. M.J. and A.J collected and processed cryo-EM data. M.J., A.J., M.L. built and refined the atomic models. M.G. and S.S. made the *C. elegans* strains and did the in vivo experiments. M.J., A.J. M.G. E.D. and N.B. wrote the manuscript. All authors contributed to the final version of this manuscript.

Funding

This work was supported by the Swiss National Science Foundation (grant number 310030B_163478), National Center of Excellence in Research RNA & Disease Program of the SNSF (grant number 51NF40_141735), and in part by the Roessler Prize, Ernst Jung Prize, and Otto Naegeli Prize for Medical Research to N.B., by research grants from the German Science Foundation (SFB969/A01, A07, and C10) to E.D. and M.G., and by the School of Medicine at the University of Virginia and the Department of Molecular Physiology and Biological Physics startup funds to A.J.

Competing Interests

The authors declare no competing interests.

bioRxiv preprint doi: https://doi.org/10.1101/2022.10.04.510795; this version posted October 4, 2022. The copyright holder for this preprint (which was not certified by peer review) is the author/funder, who has granted bioRxiv a license to display the preprint in perpetuity. It is made available under aCC-BY-NC-ND 4.0 International license.

EXTENDED DATA FIGURES

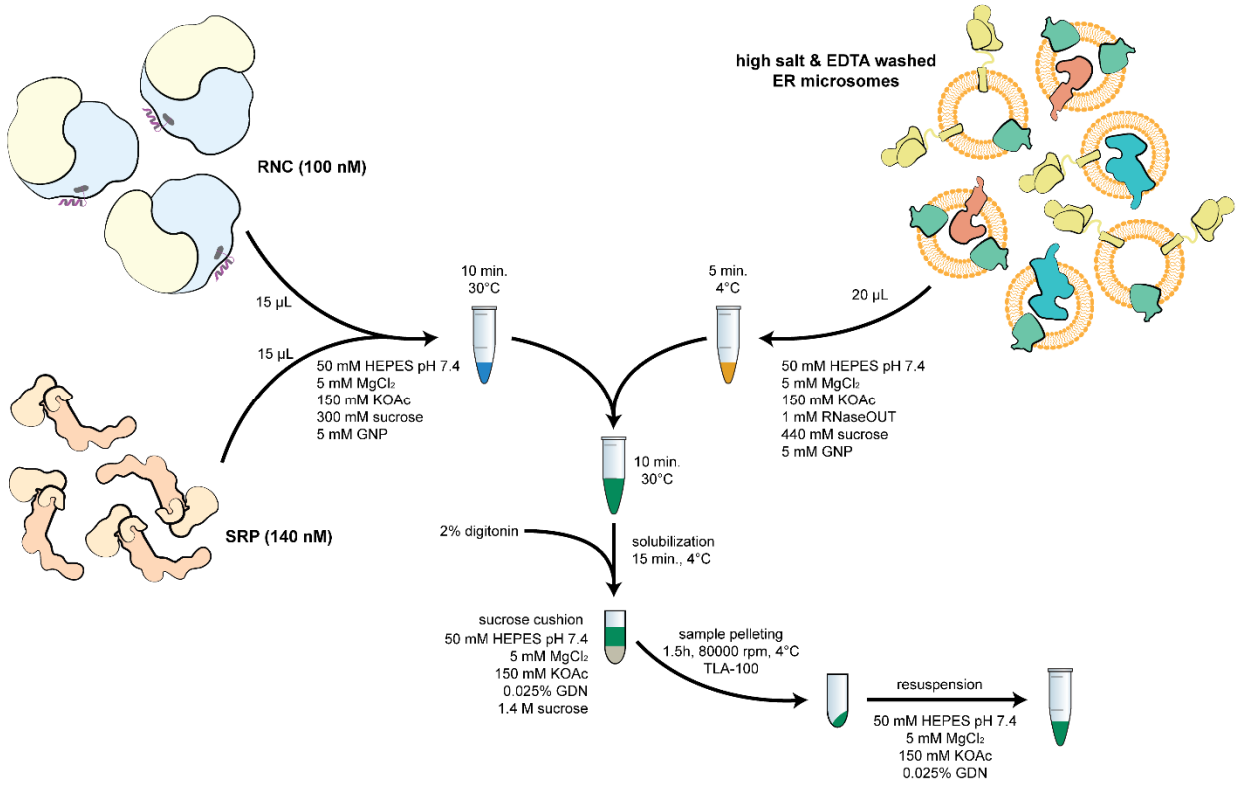

Extended Data Fig. 1 | RNC-Sec61-TRAP complex assembly.

The complex was assembled using stalled RNCs carrying an ER client mixed with canine SRP and salt- and EDTA-treated canine ER microsomes (EKRM). Microsomes were first pelleted then solubilized with 2% digitonin. Ribosome-bound complexes were then pelleted over a sucrose cushion and applied directly to cryo-EM grids.

bioRxiv preprint doi: https://doi.org/10.1101/2022.10.04.510795; this version posted October 4, 2022. The copyright holder for this preprint (which was not certified by peer review) is the author/funder, who has granted bioRxiv a license to display the preprint in perpetuity. It is made available under aCC-BY-NC-ND 4.0 International license.

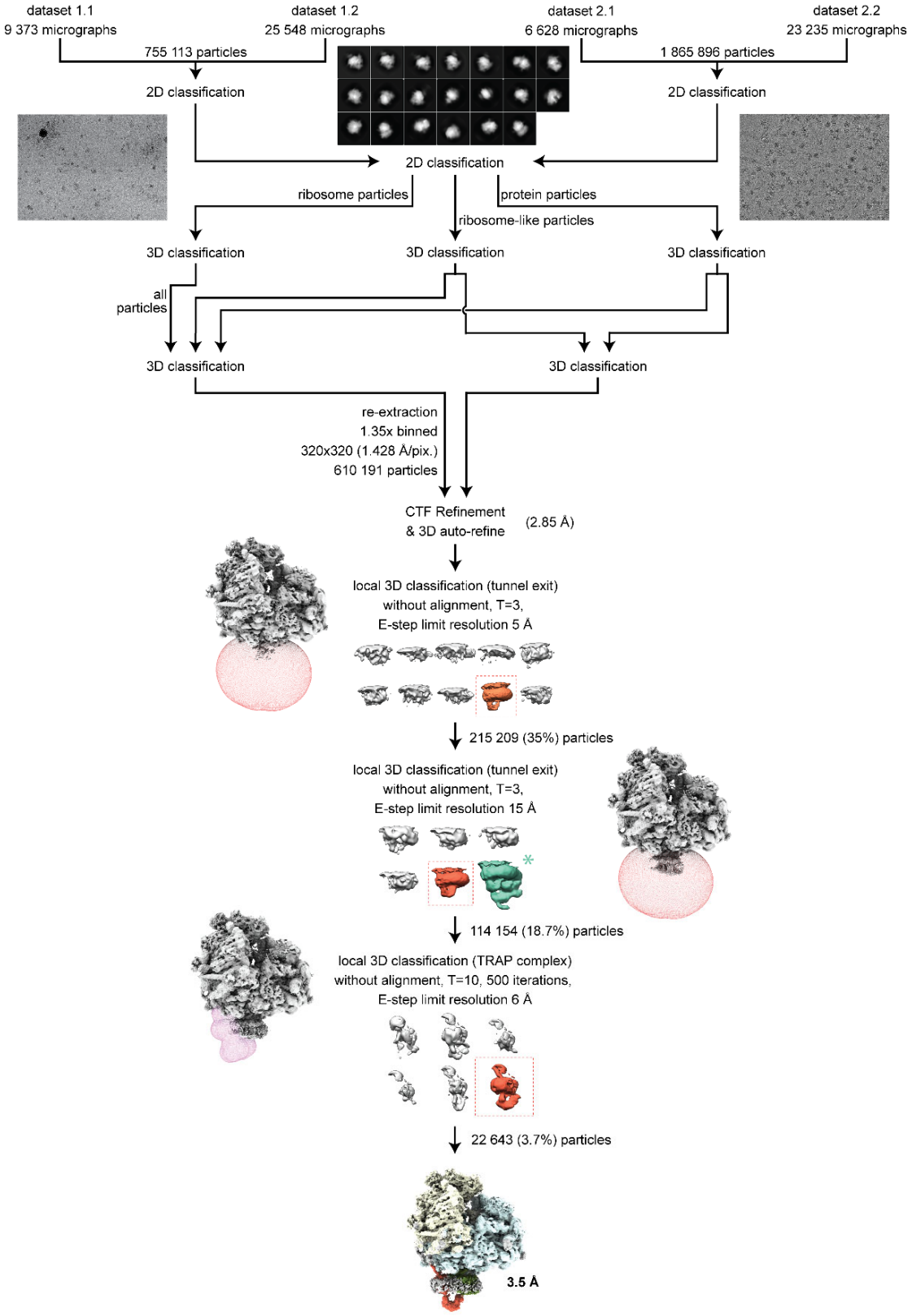

Extended Data Fig. 2 | Cryo-EM processing scheme.

bioRxiv preprint doi: https://doi.org/10.1101/2022.10.04.510795; this version posted October 4, 2022. The copyright holder for this preprint (which was not certified by peer review) is the author/funder, who has granted bioRxiv a license to display the preprint in perpetuity. It is made available under aCC-BY-NC-ND 4.0 International license.

Particles were picked from motion-corrected and dose-weighted micrographs in RELION 3.1 using lowpass filtered 80S ribosome as a reference. Particles were then exposed to two rounds of 2D classification and three rounds of 3D classification to obtain ribosome particles depicting density for the stalled P-site tRNA and the Sec61 translocon. To improve first the density of Sec61 and then TRAP complex, particles were subjected to two round of focused 3D classifications with masks applied around Sec61 and the TRAP complex. Particles (22,643) from a 3D class that depicted the strongest density for TRAP and Sec61 were refined to 3.5 Å resolution. Green asterisk indicates the complex containing OST-Sec61-TRAP complex that co-purified in the sample and was not further discussed.

bioRxiv preprint doi: https://doi.org/10.1101/2022.10.04.510795; this version posted October 4, 2022. The copyright holder for this preprint (which was not certified by peer review) is the author/funder, who has granted bioRxiv a license to display the preprint in perpetuity. It is made available under aCC-BY-NC-ND 4.0 International license.

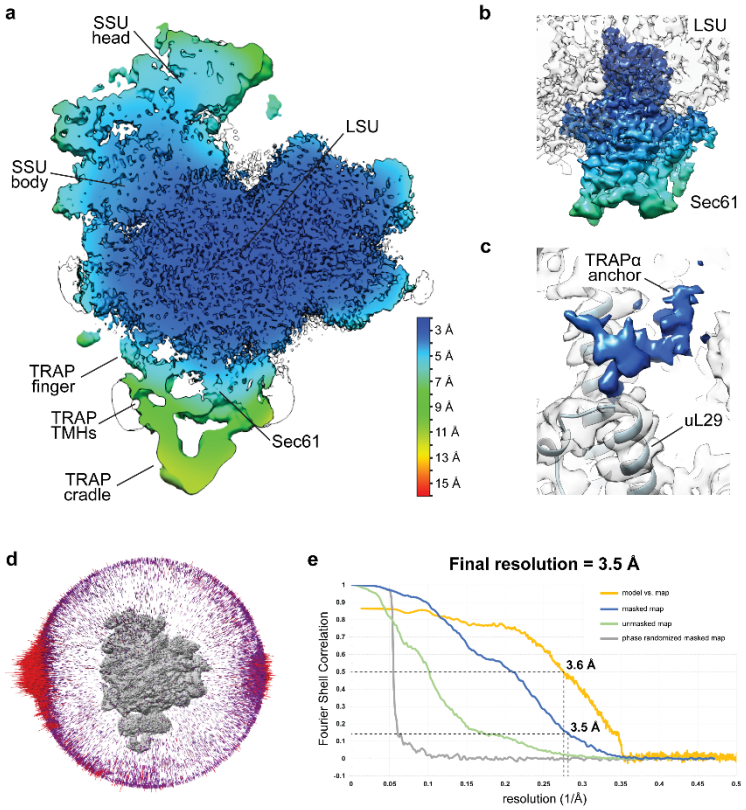

Extended Data Fig. 3 | Local Resolution and Validation Plots.

a, Local resolution of the RNC-Sec61-TRAP complex calculated in RELION 3.1. The scale bar is shown in the bottom right. **b**, Local resolution of the Sec61 translocon. Colors correspond to the same resolution as in panel (a). **c**, Local resolution of the TRAPα anchor. For clarity, ribosome density was not colored according to the local resolution. Ribosomal protein uL29 that interacts with TRAPα anchor is indicated. **d**, Angular distribution of the particles in the two cryo-EM maps after final 3D refinements. **e**, Fourier Shell Correlation (FSC) plots and the model versus map plot, calculated using the gold standard FSC criteria cutoff (FSC=0.143) using independent two half maps as implemented in RELION 3.1, and the cutoff for the resolution of the model is determined based on the FSC cutoff (FSC=0.5).

bioRxiv preprint doi: https://doi.org/10.1101/2022.10.04.510795; this version posted October 4, 2022. The copyright holder for this preprint (which was not certified by peer review) is the author/funder, who has granted bioRxiv a license to display the preprint in perpetuity. It is made available under aCC-BY-NC-ND 4.0 International license.

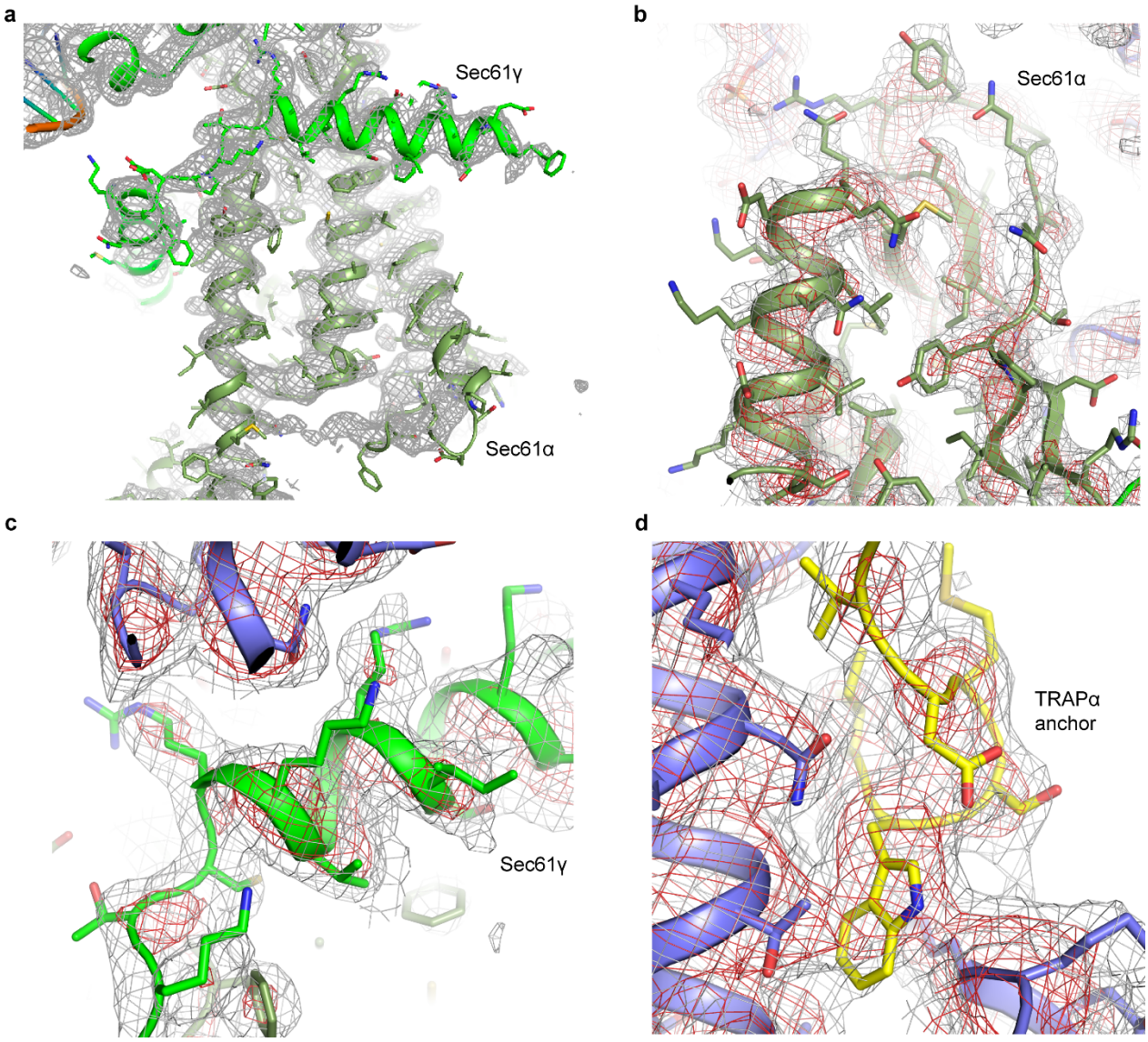

Extended Data Fig. 4 | Cryo-EM density for the high-resolution areas of Sec61 and TRAP complexes.

a-c, Cryo-EM densities corresponding to the transmembrane α-helices of the Sec61α and Sec61γ subunits. Cryo-EM density is shown as mesh and shown at two different contour levels and colored gray and red. Atomic coordinates are show as cartoon and sticks. **d**, Cryo-EM density corresponding to the TRAP anchor.

bioRxiv preprint doi: https://doi.org/10.1101/2022.10.04.510795; this version posted October 4, 2022. The copyright holder for this preprint (which was not certified by peer review) is the author/funder, who has granted bioRxiv a license to display the preprint in perpetuity. It is made available under aCC-BY-NC-ND 4.0 International license.

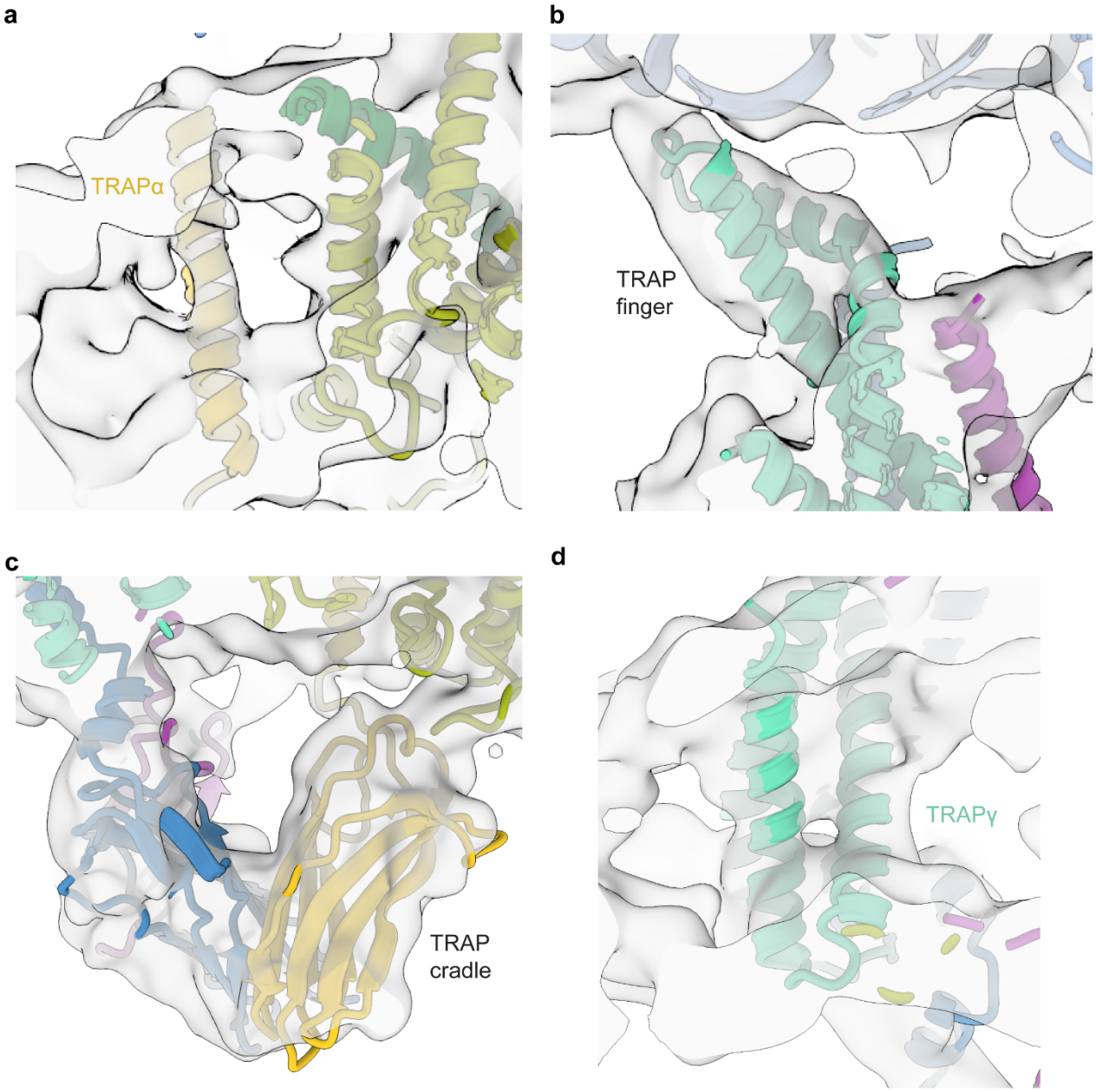

Extended Data Fig. 5 | Closeups of the TRAP complex.

a-d, Closeup cryo-EM densities of the TRAPα transmembrane helix (a), TRAP finger (b), lumenal cradle domain (c) and TRAPγ transmembrane helices (d) overlaid with atomic coordinates.

bioRxiv preprint doi: https://doi.org/10.1101/2022.10.04.510795; this version posted October 4, 2022. The copyright holder for this preprint (which was not certified by peer review) is the author/funder, who has granted bioRxiv a license to display the preprint in perpetuity. It is made available under aCC-BY-NC-ND 4.0 International license.

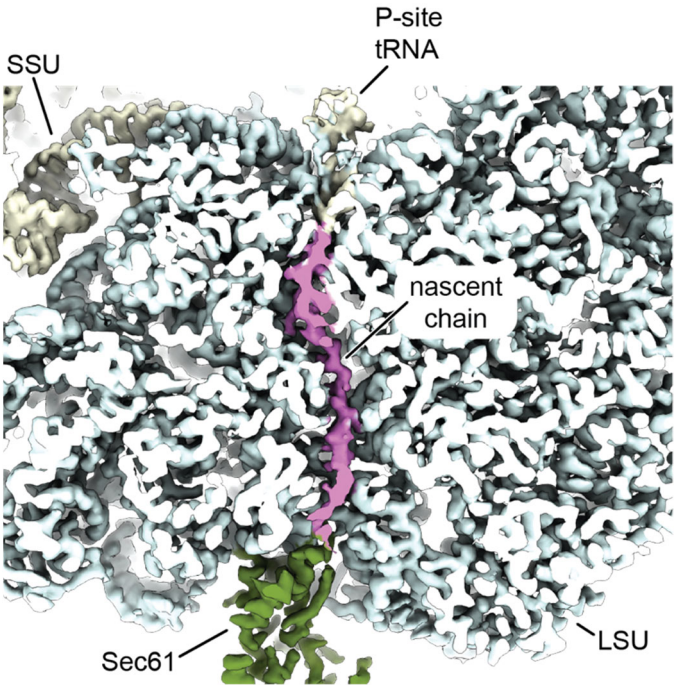

Extended Data Fig. 6 | Closeup view of the ribosome tunnel with nascent chain.

Cross section of the ribosome showing the polypeptide exit tunnel. Cryo-EM density corresponding to the nascent chain is colored in magenta. Cryo-EM density corresponding to the Sec61 complex is colored green.

bioRxiv preprint doi: https://doi.org/10.1101/2022.10.04.510795; this version posted October 4, 2022. The copyright holder for this preprint (which was not certified by peer review) is the author/funder, who has granted bioRxiv a license to display the preprint in perpetuity. It is made available under aCC-BY-NC-ND 4.0 International license.

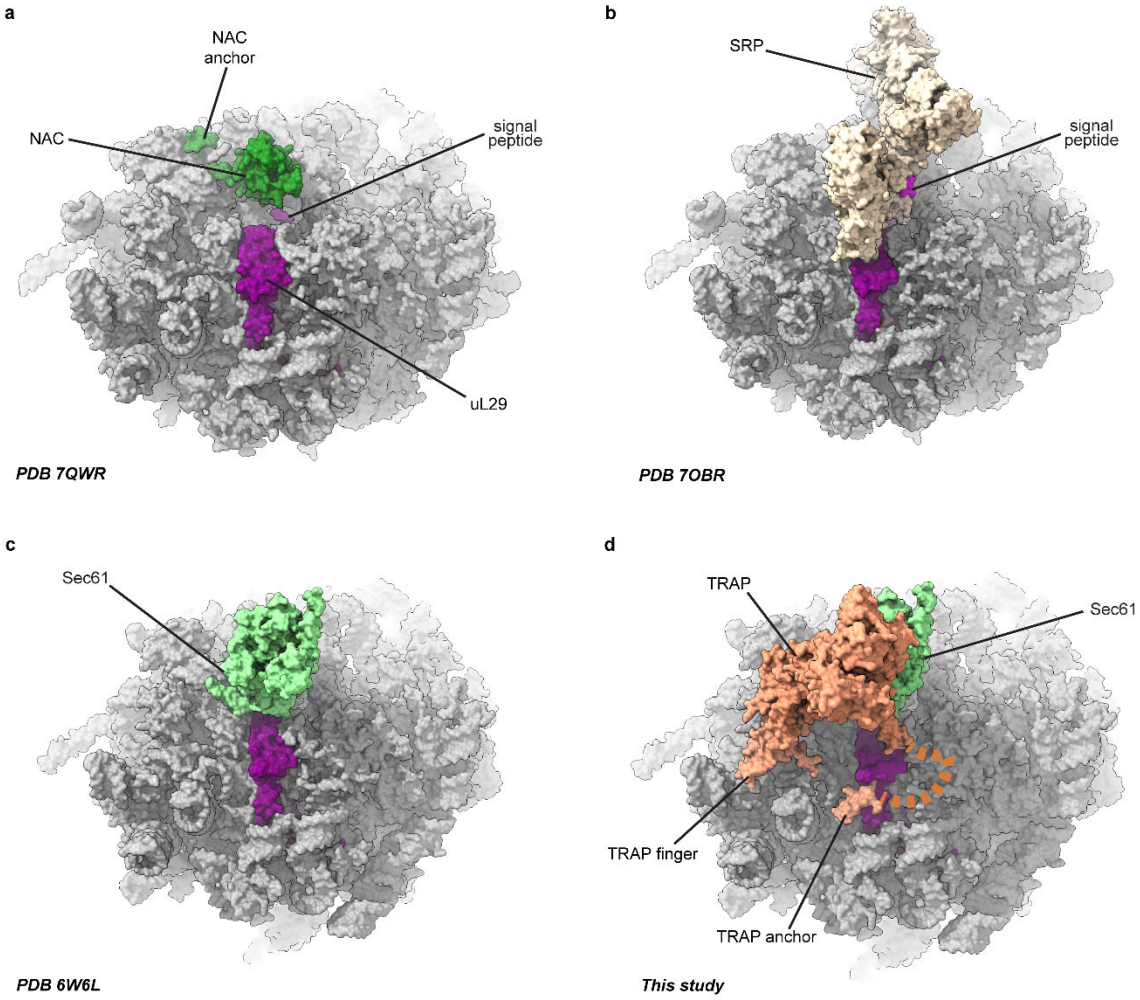

Extended Data Fig. 7 | Comparison of factors positioning at the ribosome tunnel exit.

Closeup of the ribosome tunnel exit region of the RNC-NAC (PDB 7QWR), RNC-SRP (7OBR), RNC-Sec61(6W6L) and RNC-Sec61-TRAP (this study). Atomic coordinates are shown as surface representation.

bioRxiv preprint doi: https://doi.org/10.1101/2022.10.04.510795; this version posted October 4, 2022. The copyright holder for this preprint (which was not certified by peer review) is the author/funder, who has granted bioRxiv a license to display the preprint in perpetuity. It is made available under aCC-BY-NC-ND 4.0 International license.

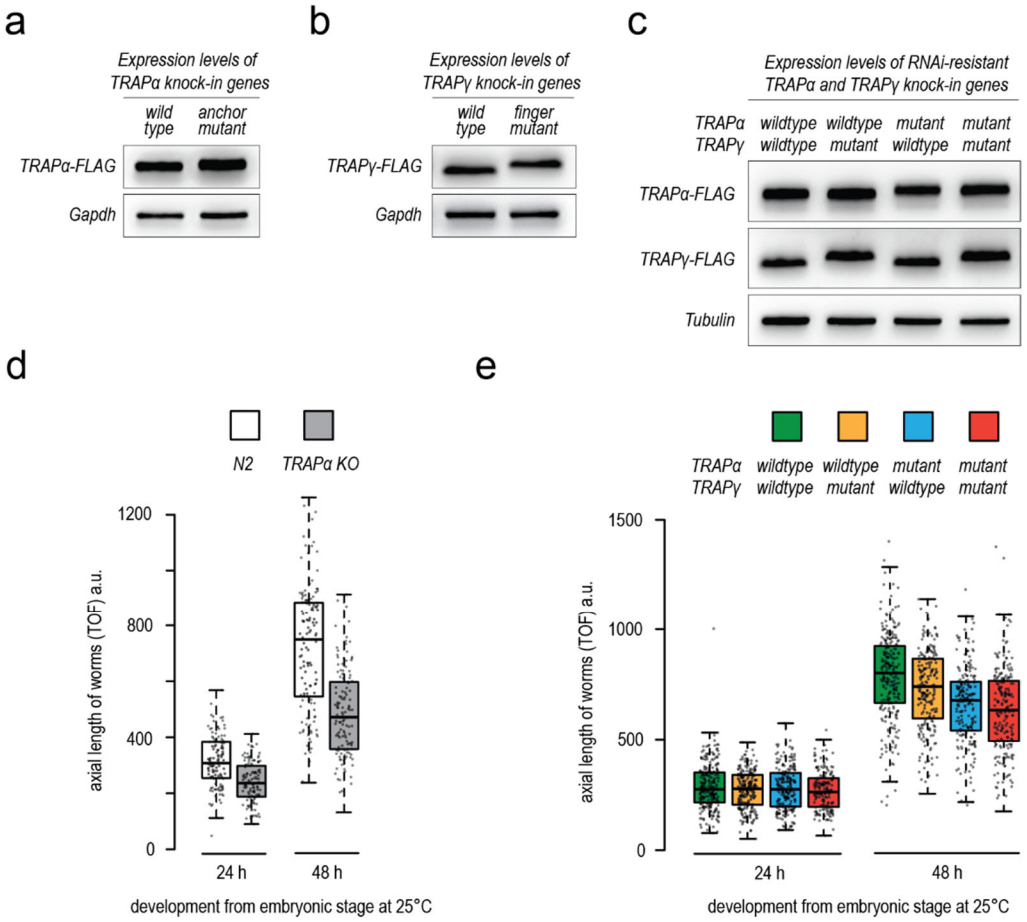

Extended Data Fig. 8 | Characterization of TRAPα and TRAPγ transgenic *C. elegans* strains.

a-c, FLAG immunoblot analysis showing the TRAPα and TRAPγ expression levels in worms analyzed in main Fig. 2d, g, and h, respectively. All TRAP variants were tagged with a C-terminal mono-FLAG tag. Gapdh or Tubulin served as loading control. **d,** Growth analysis of wildtype N2 and TRAPα knockout worms. Worms were synchronized via a timed egg-lay and plates incubated for the indicated time at 25°C. The axial length of worms was determined by worm flow cytometry using a COPAS Biosorter. Box plot center line indicates the median, box length the upper and lower quartile, and whiskers the minimum/maximum quartile ($n \geq 125$). Dots represent individual data points. TOF, time-of-flight. a.u., arbitrary units. **e,** Similar analysis as in panel d with worms expressing indicated RNAi-resistant TRAPα and TRAPγ transgenes. Analysis was performed in the endogenous TRAPα and TRAPγ RNAi background (F2 RNAi generation).

bioRxiv preprint doi: https://doi.org/10.1101/2022.10.04.510795; this version posted October 4, 2022. The copyright holder for this preprint (which was not certified by peer review) is the author/funder, who has granted bioRxiv a license to display the preprint in perpetuity. It is made available under aCC-BY-NC-ND 4.0 International license.

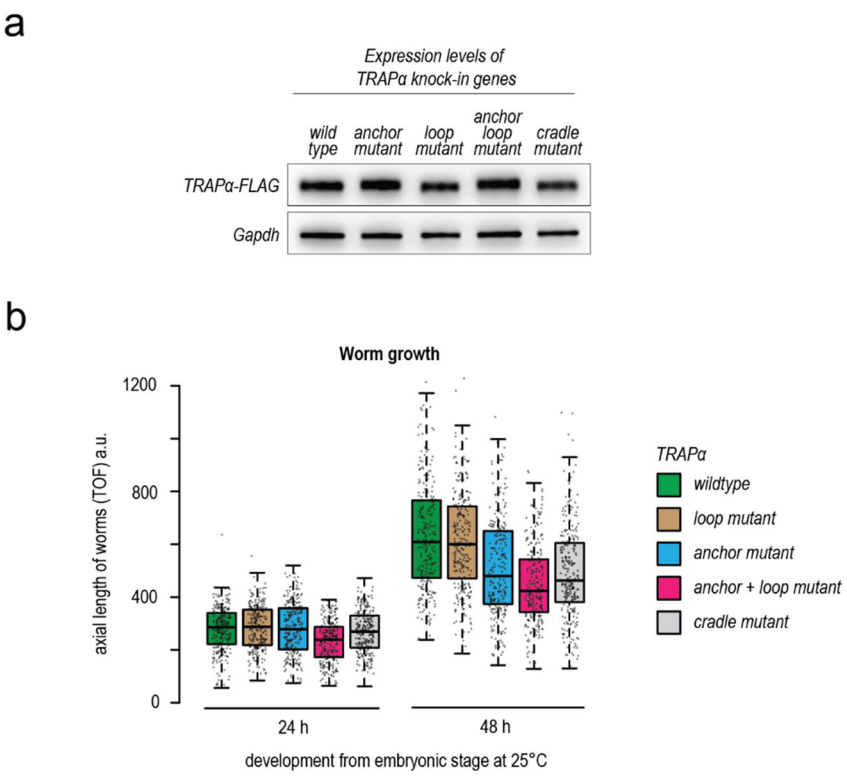

Extended Data Fig. 9 | Characterization of TRAPα KO complemented worms.

a, FLAG immunoblot analysis showing expression levels of indicated TRAPα variants in C. elegans worms analyzed in main Fig. 3. The different TRAPα variants are tagged with a C-terminal mono-FLAG tag. Gapdh served as loading control. **b,** Growth analysis of TRAPα knockout worms complemented with indicated TRAPα transgenes. Worms were synchronized via a timed egg-lay and plates incubated for the indicated time at 25°C. The axial length of worms was determined by worm flow cytometry using a COPAS large particle Biosorter. Box plot center line indicates the median, box length the upper and lower quartile, and whiskers the minimum/maximum quartile ($n \geq 250$). Dots represent individual data points. TOF, time-of-flight. a.u., arbitrary units.

bioRxiv preprint doi: https://doi.org/10.1101/2022.10.04.510795; this version posted October 4, 2022. The copyright holder for this preprint (which was not certified by peer review) is the author/funder, who has granted bioRxiv a license to display the preprint in perpetuity. It is made available under aCC-BY-NC-ND 4.0 International license.

Extended Data Table 1 | EM data collection and structure refinement statistics.

	80S nascent chain complex with TRAP and Sec61
EMDB code	####
PDB code	####
Data collection and processing	
Magnification	81,000x (nominal)
Voltage (kV)	300
Electron exposure (e^{-}/Å^2)	60
Defocus range (μm)	0.6-3.0
Pixel size (Å)	1.06 (super-resolution pixel at 0.53Å/pixel)
Initial particle images (no.)	2,621,009
Final particle images (no.)	22,643
Map resolution at FSC=0.143 (Å)	3.5
Structure refinement in PHENIX 1.20.1	
Model resolution at FSC=0.5 (Å)	3.7
CC_{mask}	0.75
Map sharpening B factor (Å^2)	– 63.5
Model composition	
Non-hydrogen atoms	233,824
Protein residues	13,272
RNA residues	5,890
Ligands: Mg^{2+}/Zn^{2+}/SPM/SPD	750/8/330/3/30
B factors min/max/mean (Å^2)	
Protein	14/348/139
RNA	6/693/171
Ligand	6/341/93
RMSD	
Bond lengths (Å)	0.001
Bond angles (°)	0.344
Validation	
MolProbity score	1.3
Clashscore	5.61
Poor rotamers (%)	0.8
Protein	
EM Ringer score	1.9
Ramachandran plot	
Favored (%)	98.69
Allowed (%)	1.29
Disallowed (%)	0.02
RNA	
Pucker outliers (%)	0.05
Bond outliers (%)	0.09
Angle outliers (%)	0.0
Suite outliers (%)	12.1

CC_{mask}, real space correlation coefficients; EMDB, Electron Microscopy Data Bank; FSC, Fourier shell correlation; PDB, Protein Data Bank; RMSD, root-mean-square deviation; SPM, spermine; SPD, spermidine,

bioRxiv preprint doi: https://doi.org/10.1101/2022.10.04.510795; this version posted October 4, 2022. The copyright holder for this preprint (which was not certified by peer review) is the author/funder, who has granted bioRxiv a license to display the preprint in perpetuity. It is made available under aCC-BY-NC-ND 4.0 International license.

Extended Data Table S2

Table S2. Sequence of synthetic RNAi-resistant wildtype TRAPα gene (*syn-trap-1*)
ATGAAGCTTTCCACCGTCTTCCTCCTTGCTGCCCTCGGATTCTGCGCCGTCTACGCT GCTGATGTTGTCGATGGAGAGGTCACCGACGATGCTCCAAAGAACTCTCAAGAGG ATGACGACCTTACCATCGGAGCTTCCCCAGACGCTGGACTCGCTTTCCACTTCGTC CAACCATCCGACGCTAACGTCGTCCGTGAATTCTACACTGGAAAGCCAGTTAAGTA CCTTATCGGATTCCAGgtaagtttaaacatatatatactaactaaccctgattatttaaattttcagAACAAGGGAGA GAAGGATTTCGTTGTTAAGTACGCCGAGACCTCCTTCCGCTTCCCAACCGACCACT CTTACCACCTTCAAAACTTCACCCGTGGAGAGTACAACCGTCGTGTTGCTCCAAAG gtaagtttaaacagttcggtactaactaaccatacatatttaaattttcagGAGGAGGTTACCCTTGATTACGGATT CTACGCTCACGAAACCTTCGCTGGACGTCCAGTCGGACTTGTTGTTAACGTCCACT ACCAAGATGCTGATGGAAACGTCTTCGTTAACAACGTTTACAACCAAACTATCAAC ATCATGGAGGATGATTCCGGATTCTCCGGAGAGACTGGATTCCTTTTCATTTTCTTC GTCGCTCTTTCCATCGGAGGACTTTACCTCTCTAACCAATTCCTCTCTAAGCTTTCT CGTAAGTCCGGACTTTCCAAGCGTCGTGTCGTCGAGCAAGGAACCTCTTCTGAGGT TGATTTCGAGTGGATCCCACGCGACGCTGTTAAGgtaagtttaaacatgattttactaactaactaatctgat ttaaattttcagAACAAGGAGAAGCGCTCTCCAGCTACCGTTTCTCCAAAGGCCCGTAAGT CCGCTAAGAAGGCCGACGATTATAAAGATGATGATGATAAATAA

Lower case = synthetic introns. Grey = FLAG tag.

bioRxiv preprint doi: https://doi.org/10.1101/2022.10.04.510795; this version posted October 4, 2022. The copyright holder for this preprint (which was not certified by peer review) is the author/funder, who has granted bioRxiv a license to display the preprint in perpetuity. It is made available under aCC-BY-NC-ND 4.0 International license.

Extended Data Table S3

Table S3. Sequence of synthetic RNAi-resistant wildtype TRAPγ gene (*syn-trap-3*)
ATGGGAAAGCTTACTAAGGAGGAGGAGCTCCTTCTTTCTTCTTACTCTGCTACCTC TTCTACTAAGgtaagtttaaacatatatatactaactaaccctgattatttaaattttcagGGAAATCTTTTCTTCTAC CTTAACGCTCTTATCATCTCCATCGCTCCACTTTACCTTTTCTACGGAGTCCATCAA ATGGAGATCCAAGATTCTCTCGTCGTCTGGGGACTTTCCGCTGTCGGAACCGCTTA CCTTCTTTCCCTTGCTTGCAAGAACCAAAAGTGCCTCCTTAAGCACCAAATCGTTA TGAAGCGTGGATCCGCCGTTGAGCGTGAGATCTCTGGACAATACGCCGCCGATAA GgtaagtttaaacagttcggtactaactaaccatacatatttaaattttcagAAGATGACCGTCAAGGAGAAGGAG GAGCGTGCTCTCTTCCGTAAGgtaagtttaaacatgattttactaactaactaatctgatttaaattttcagAACGAG GTTGCTGATACCGAGTCTACCTACCTTTCTGTTTTCTACACCAACTCTCTTTACCTT ACCATCATGCTTGTCTCCGCTTTCTTCCTTCTTGCTAACGTTGCCCCAGTCTTCAAC CTTCTTATCTCTACCATCGGATCCGCTGGACTTGTCGCTTTCCTTTCCACCGCCAAG AACGATTATAAAGATGATGATGATAAATAA

Lower case = synthetic introns. Grey = FLAG tag.

bioRxiv preprint doi: https://doi.org/10.1101/2022.10.04.510795; this version posted October 4, 2022. The copyright holder for this preprint (which was not certified by peer review) is the author/funder, who has granted bioRxiv a license to display the preprint in perpetuity. It is made available under aCC-BY-NC-ND 4.0 International license.

Extended Data Table S4

Table S4	***C. elegans* strains**
DEU156	gamSi56 [*trap-1p::WT-syn-trap-1-FLAG*; *icd-2p::mCherry*]
DEU157	gamSi57 [*trap-1p::W228A-K239E-K235E-syn-trap-1-FLAG*; *icd-2p::mCherry*]
DEU158	gamSi58 [*trap-1p::*^{133}HETFAGR/SSSSSSS^{139}*-syn-trap-1-FLAG*; *icd-2p::mCherry*]
DEU159	gamSi59 [*trap-1p::*^{133}HETFAGR/SSSSSSS^{139}*-W228A-K239E-K235E-syn-trap-1-FLAG*; *icd-2p::mCherry*]
DEU160	gamSi60 [*trap-1p::F98T-Y104T-L106T-F109T-L126T-Y128T-Y131T-V141T-syn-trap-1-FLAG*; *icd-2p::mCherry*]
DEU161	gamSi61 [*trap-3p::WT-syn-trap-3-FLAG*; *icd-2p::mCherry*]
DEU162	gamSi62 [*trap-3p::K103E-K104E-K108E-syn-trap-3-FLAG*; *icd-2p::mCherry*]
DEU163	trap-1(gk5960); zcIs4 [*hsp-4p::GFP*; *loxP* + *myo-2p::GFP* + *rps-27p::neoR* + *loxP*]
DEU164	trap-1(gk5960); zcIs4; gamSi56 [*hsp-4p::GFP*; *loxP* + *myo-2p::GFP* + *rps-27p::neoR* + *loxP; trap-1p::WT-syn-trap-1-FLAG; icd-2p::mCherry*]
DEU165	trap-1(gk5960); zcIs4; gamSi57 [*hsp-4p::GFP*; *loxP* + *myo-2p::GFP* + *rps-27p::neoR* + *loxP; trap-1p::W228A-K239E-K235E-syn-trap-1-FLAG; icd-2p::mCherry*]
DEU166	trap-1(gk5960); zcIs4; gamSi58 [*hsp-4p::GFP*; *loxP* + *myo-2p::GFP* + *rps-27p::neoR* + *loxP; trap-1p:* ^{133}HETFAGR/SSSSSSS^{139}*-syn-trap-1-FLAG; icd-2p::mCherry*]
DEU167	trap-1(gk5960); zcIs4; gamSi59 [*hsp-4p::GFP*; *loxP* + *myo-2p::GFP* + *rps-27p::neoR* + *loxP; trap-1p::*^{133}HETFAGR/SSSSSSS^{139}*-W228A-K239E-K235E -syn-trap-1-FLAG; icd-2p::mCherry*]
DEU168	trap-1(gk5960); zcIs4; gamSi60 [*hsp-4p::GFP*; *loxP* + *myo-2p::GFP* + *rps-27p::neoR* + *loxP; trap-1p::F98T-Y104T-L106T-F109T-L126T-Y128T-Y131T-V141T-syn-trap-1-FLAG; icd-2p::mCherry*]
DEU169	zcIs4; gamSi61 [*hsp-4p::GFP*; *trap-3p::WT-syn-trap-3-FLAG*; *icd-2p::mCherry*]
DEU170	zcIs4; gamSi62 [*hsp-4p::GFP*; *trap-3p::K103E-K104E-K108E-syn-trap-3-FLAG*; *icd-2p::mCherry*]
DEU171	zcIs4; gamSi56; gamSi61 [*hsp-4p::GFP*; *trap-1p::WT-syn-trap-1-FLAG; trap-3p::WT-syn-trap-3-FLAG*; *icd-2p::mCherry*]
DEU172	zcIs4; gamSi56; gamSi62 [*hsp-4p::GFP*; *trap-1p::WT-syn-trap-1-FLAG; trap-3p::K103E-K104E-K108E-syn-trap-3-FLAG*; *icd-2p::mCherry*]
DEU173	zcIs4; gamSi57; gamSi61 [*hsp-4p::GFP*; *trap-1p::W228A-K239E-K235E-syn-trap-1-FLAG; trap-3p::WT-syn-trap-3-FLAG*; *icd-2p::mCherry*]
DEU174	zcIs4; gamSi57; gamSi62 [*hsp-4p::GFP*; *trap-1p::W228A-K239E-K235E-syn-trap-1-FLAG; trap-3p::K103E-K104E-K108E-syn-trap-3-FLAG*; *icd-2p::mCherry*]
DEU175	daf-2(e1368); trap-1(gk5960) [daf-2(e1368) III.; *loxP* + *myo-2p::GFP* + *rps-27p::neoR* + *loxP*]

bioRxiv preprint doi: https://doi.org/10.1101/2022.10.04.510795; this version posted October 4, 2022. The copyright holder for this preprint (which was not certified by peer review) is the author/funder, who has granted bioRxiv a license to display the preprint in perpetuity. It is made available under aCC-BY-NC-ND 4.0 International license.

DEU176	daf-2(e1368); trap-1(gk5960); gamSi56 [daf-2(e1368) III.; *loxP + myo-2p::GFP + rps-27p::neoR + loxP; trap-1p::WT-syn-trap-1-FLAG*; *icd-2p::mCherry*]
DEU177	daf-2(e1368); trap-1(gk5960); gamSi57 [daf-2(e1368) III.; *loxP + myo-2p::GFP + rps-27p::neoR + loxP; trap-1p::W228A-K239E-K235E-syn-trap-1-FLAG*; *icd-2p::mCherry*]
DEU178	daf-2(e1368); trap-1(gk5960); gamSi60 [daf-2(e1368) III.; *loxP + myo-2p::GFP + rps-27p::neoR + loxP; trap-1p::F98T-Y104T-L106T-F109T-L126T-Y128T-Y131T-V141T-syn-trap-1-FLAG*; *icd-2p::mCherry*]